Electronic Theses and Dissertations

Theses, Dissertations, and Major Papers

9-7-2018

Impact of Front-end Air Flow Conditions on AC Performance and Real-World Fuel Economy

Keyuan Yang
University of Windsor

Follow this and additional works at: https://scholar.uwindsor.ca/etd

**Impact of Front-end Air Flow Conditions on
AC Performance and Real-World Fuel Economy**

by

Keyuan Yang

A Thesis
Submitted to the Faculty of Graduate Studies
through the Department of Mechanical, Automotive & Materials Engineering
in Partial Fulfillment of the Requirements for
the Degree of Master of Applied Science
at the University of Windsor

Windsor, Ontario, Canada

2018

Impact of Front-end Air Flow Conditions on
AC Performance and Real-World Fuel Economy

by

Keyuan Yang

APPROVED BY:

_____

J. Defoe

Mechanical, Automotive & Materials Engineering

_____

A. Edrisy

Mechanical, Automotive & Materials Engineering

_____

D. Ting, Advisor

Mechanical, Automotive & Materials Engineering

8/29/2018

DECLARATION OF ORIGINALITY

I hereby certify that I am the sole author of this thesis and that no part of this thesis has been published or submitted for publication.

I certify that, to the best of my knowledge, my thesis does not infringe upon anyone's copyright nor violate any proprietary rights and that any ideas, techniques, quotations, or any other material from the work of other people included in my thesis, published or otherwise, are fully acknowledged in accordance with the standard referencing practices. Furthermore, to the extent that I have included copyrighted material that surpasses the bounds of fair dealing within the meaning of the Canada Copyright Act, I certify that I have obtained a written permission from the copyright owner(s) to include such material(s) in my thesis and have included copies of such copyright clearances to my appendix.

I declare that this is a true copy of my thesis, including any final revisions, as approved by my thesis committee and the Graduate Studies office, and that this thesis has not been submitted for a higher degree to any other University or Institution.

ABSTRACT

Active grille shutter (AGS) in a vehicle provides aerodynamic benefit at high vehicle speed by closing the front-end grille opening. At the same time, this causes lesser air to flow through the cooling module which includes the condenser. This results in a higher head pressure (AC compressor discharge pressure of the refrigerant). Higher head pressure causes the compressor to work more thereby possibly negating the aerodynamic benefits. This thesis shows a model-based method to quantify the fuel consumption in different scenarios to justify the AGS position (fully open or fully closed) to have better fuel economy.

The impact of AGS is more felt at highway speed, so the AGS will be open at low speed or idle. This thesis focuses on the tradeoff between the aerodynamic performance and the compressor power consumption at high vehicle speeds and mid-ambient conditions (26.7°C and 32.2°C).

The results from the steady-state simulations show a tiny reduction in the fuel consumption rate for AGS closed condition by comparing to AGS open condition; while the results for the transient cycle show a remarkable reduction in the fuel consumption rate when the vehicle reaches the highest speed of 128.7 km/h. However, at the low-speed range, there is no benefit in fuel economy with AGS closed, as expected.

ACKNOWLEDGEMENTS

TABLE OF CONTENTS

LIST OF FIGURES

LIST OF TABLES

LIST OF ABBREVIATIONS

AC—air conditioning

AGS—active grille shutter

CCD—cabin cool-down test

CDP—compressor discharge pressure

CFC—cumulated fuel consumption

CFD—computational fluid dynamics

COP—coefficient of performance

FCR—fuel consumption rate

HEAT—heat exchangers assembly tool

HVAC—heating, ventilation, and air conditioning

IHX—internal heat exchanger

TPF—two phase flow

TXV—thermal expansion valve

VDC—variable displacement compressor

LIST OF NOMENCLATURE

Upper and lower case

A   Area [m²]

$A_{frontal}$ Frontal area

a   Nusselt number constant

b   Nusselt number constant

c   Nusselt number constant

c_p Constant pressure specific heat [kJ/(kg·K)]

C   Thermal capacity [kJ/K]

Cd   Coefficient of drag

g   Gravitational acceleration [m/s²]

h   Specific enthalpy [kJ/kg]

ℏ   Convection coefficient [W/(m²·K)]

L_c Characteristic length [m]

M   Mass [kg]

$\dot{m}$ Mass flow rate [kg/s]

N   Compressor speed [rpm]

P   Pressure [Pa]

$\dot{Q}$ Heat transfer rate [W]

R   Specific gas constant for dry air [J/(kg·K)]

S   Displacement of the piston [cc]

t   Thickness [m]

T   Torque [Nm]

T	Temperature [K]
v	Velocity [m/s]
V	Volume [m^3]
$\dot{V}$	Volume flow rate [m^3/s]

Greek

ρ	Density [kg/m3]
η	Efficiency
Δ	Finite change in quantity

Subscription

disc	Discharge
ext	External
ref	Reference
mech	Mechanical
sim	Simulation
suct	Suction
s	Surface
v	Volumetric

CHAPTER 1 INTRODUCTION

As the legislation on fuel consumption gets more stringent over time, the whole automotive industry is giving their best effort to improve fuel economy from every possible aspect. According to the emission reduction targets for new cars set by European Union legislation, the CO2 emission should reduce to 95 grams per kilometers by 2021 [1]. By comparing to the average emission level of new cars sold in 2016, the reduction is about 24%. The US Congress also established Corporate Average Fuel Economy (CAFE) standards under the Energy Policy and Conservation Act, to regulate the greenhouse emission and fuel economy standards for light-duty trucks, passenger cars and medium-duty passenger vehicles [2]. The final standards planned to result in an average level of 163 grams per mile of carbon dioxide in model year 2025. Advanced technological solutions must be developed to reduce fuel consumption to achieve sustainability.

Over half of the energy in vehicles is lost to different cooling systems which include the engine cooling system, air conditioning system (AC), frictional components cooling, and exhaust gas [3]. Improving the efficiency of the air conditioning system will reduce the power consumed by the compressor, hence the load on the engine. To achieve this goal, engineers worked on improving the efficiency of the heat exchangers, and later they introduced internal heat exchanger which improves the cooling performance of the AC system up to 7% with refrigerant R1234yf [4]. On the other hand, improving aerodynamic performance is another way to achieve better fuel economy. Engineers have spent decades to design the perfect shape of vehicles to reduce aerodynamic drag. Recently, a technology called active grille shutter (AGS) is becoming popular in the automotive industry. The AGS is a special shutter which is installed in front of the cooling package of the vehicle. It can be opened and closed according to the vehicle operating conditions to reduce aerodynamic resistance. While the AGS is entirely closed, the air flows around the vehicle body, the resistance is reduced which improves the aerodynamic performance. However, the air flowing through the condenser will not be sufficient; the AC system will consume more power to achieve the same cooling performance. Apparently, there is a trade-off between the aerodynamic performance and the AC cooling performance. During the last decade, a few researchers have investigated the impact of AGS on the engine cooling and the HVAC system. Half of the work was done experimentally which requires the actual vehicle, the experimental setup, and all the measuring devices. The presented thesis introduces a model-based process which can evaluate the impact of an AGS on the vehicle before testing the prototype. The

objective is to investigate the effect of various air flow conditions, corresponding to different AGS positions (fully open and fully closed), on the AC performance and fuel economy. By comparing the fuel consumed with AGS open and ASG closed, the AGS position can be justified to ensure lower fuel consumption.

1.1 Vapor-compression cycle

The ideal vapor-compression cycle is the most widely used cycle for refrigerators, air conditioning systems and heat pumps. The cycle has four main components: a compressor, a condenser, a thermal expansion valve and an evaporator. In the beginning of this process, the refrigerant enters the compressor as saturated vapor, the vapor is then compressed and passes through the condenser while releasing heat to the surrounding, and the refrigerant flows out as saturated liquid. Then the refrigerant is throttled to evaporator pressure by the thermal expansion valve, the temperature of the vapor-liquid mixture also drops below the temperature of the refrigerated space. While it passes through the evaporator, the heat is absorbed from the refrigerated area and the refrigerant becomes saturated vapor again at the exit and reenters the compressor. Since the heat is taken away from the air, the temperature drops in the refrigerated area. The cycle is demonstrated below in Figure 1-1. The whole cycle can be summarized into four processes:

1-2 Isentropic compression in a compressor

2-3 Constant-pressure heat rejection in a condenser

3-4 Throttling in an expansion device

4-1 Constant-pressure heat absorption in an evaporator

A compressor inside an AC system is a device that increases the pressure of the refrigerant by reducing the volume. There are two most commonly used types of the compressor in automobile AC systems, which are fixed displacement compressor and variable displacement compressor. In this work, a swash plate variable displacement compressor is used. The variable displacement compressor is controlled to adjust its stroke according to the cooling load to minimize the power consumption; it is widely used in the automotive industry today. Nowadays, the condenser in the AC system usually comes with an integrated receiver-dryer. The receiver-dryer is located between the third and the fourth pass in a four-pass condenser. The primary function of this device is to receive and serve as temporary storage for excess liquid refrigerant. There is always excess refrigerant stored in the receiver to compensate for the leakage during the lifetime usage.

When the system is under low cooling demand, a fraction of the refrigerant is needed; the excess refrigerant will remain inside the receiver. Another function is to remove water from the refrigerant. In this way, it prevents partial freezing in thermal expansion valve (TXV) during the engine start-up stage [4].

The condenser and the evaporator are the two heat exchangers in the AC system. In the condenser, the refrigerant with high pressure and high temperature rejects heat to the ambient air outside the vehicle. During this process, the superheated vapor enters the condenser at the top and leaves as a subcooled liquid at the bottom. The condenser is located at the front of the vehicle, where steady air flow can be achieved when the vehicle is at high speeds. However, during idle or at low vehicle speed, there is a fan system to enhance the air flow and improve the heat removal process. The performance of the condenser is mostly dependent on the air flow, since the air flow rate determines the convective heat transfer coefficient which represents the efficiency of the heat exchange process between the air flow and the condenser. The typical configurations of condensers are plate and fin and serpentine fin and parallel flow type. The evaporator has a similar construction to the condenser, but instead of dumping unwanted heat, the evaporator absorbs heat from the refrigerated area as the air flows through the evaporator. At the inlet of the evaporator, the refrigerant is a mixture of liquid and gas with low pressure and low temperature, as the refrigerant absorbs energy from the air that will enter the refrigerated space, it becomes saturated vapor and then superheated vapor during this process. In the present thesis, a dual AC system is used, which means there are two evaporators, one in the front and one in the rear.

The TXV, which is located between the condenser and the evaporator, is a metering device that controls the volume flow rate of the refrigerant. There are three primary functions of TXV: to divide the system into high-pressure and low-pressure side; to meter the refrigerant flow rate and hence control the evaporator cooling capacity; to ensure that there is superheated vapor at the exit and the entire liquid refrigerant has been vaporized in the evaporator. To achieve the last two functions, the TXV can sense the refrigerant temperature at the exit of the evaporator. If the temperature is too low, which means the cooling load is also low, the TXV reduces its opening and lets less refrigerant pass through to ensure that the entire refrigerant can be vaporized at the exit.

In this thesis, an IHX is also included in the AC system. This device is used to improve the cooling capacity by utilizing the energy that is otherwise wasted. The internal heat exchanger is installed between the condenser and the evaporator, as the hot liquid refrigerant from the condenser flows into the IHX and releases heat to the cool refrigerant vapor from the evaporator,

the liquid refrigerant is further cooled below the condensation temperature. Thereby, the refrigerant is able to absorb more energy from the indoor air as it passes through the evaporator and the cooling effect of the AC system is improved. More details of the AC components can be found in 3.2 of this work.
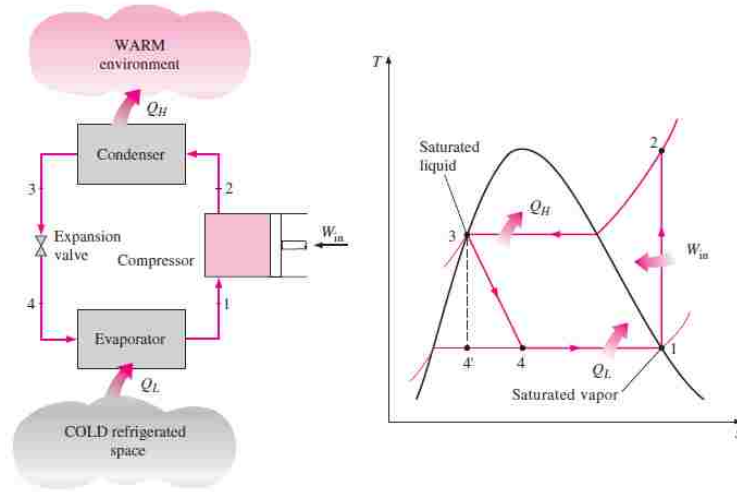
Figure 1-1: Schematic and T-s diagram for the ideal vapor-compression refrigeration cycle, from Cengel [6].
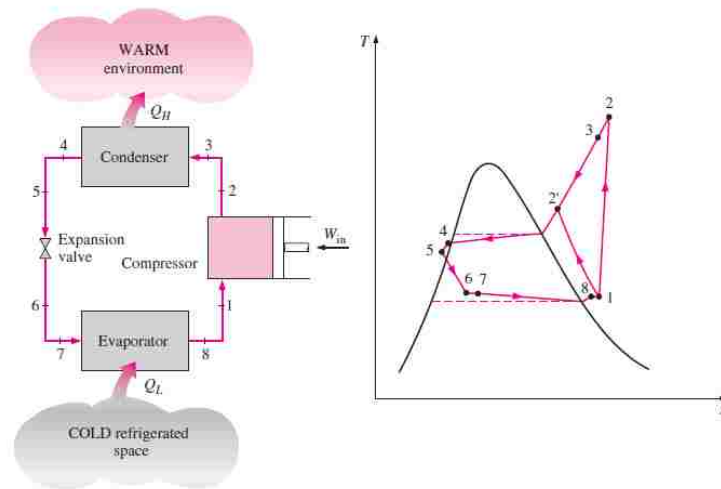
Figure 1-2: Schematic and T-s diagram for the actual vapor-compression refrigeration cycle, from Cengel [6].

The T-s diagram for an actual vapor compression cycle is shown in Figure 1-2. The actual cycle differs from the ideal cycle due to the irreversibility that occurs in several components. The pressure loss due to friction and the heat transfer to or from the surroundings is the common source [5]. Also, it is not possible to ensure saturated vapor entering the compressor in real life, in

fact, the vapor is superheated to make sure no liquid enters the compressor. Similarly, the refrigerant leaves the condenser as a subcooled liquid in the actual cycle instead of saturated liquid, so that as it enters the evaporator, it can absorb more energy from the surrounding due to its low enthalpy.

1.2   Active grille shutter

An AGS is a special shutter in the grille that opens and closes automatically to reduce aerodynamic drag and ultimately the fuel consumption. Usually, the AGS will be fully closed at highway speed, so the air flows around the vehicle instead of flowing into the engine compartment, the aerodynamic drag will be less when compared with AGS open condition. It offers several other advantages such as lower engine noise, faster engine and cabin warm-up in cold conditions. However, in hot ambient conditions, while the AC system is operating, it is necessary to consider the effect of the insufficient air flows through the AC condenser when the AGS is closed. In this case, the AC system will require more power to achieve the same cooling performance. The AC system is one of the largest auxiliary loads in vehicles; the power increment could overtake the advantage that is provided by the AGS in the closed condition. There is a tradeoff between the AC performance and the aerodynamic performance. Since the final objective is to improve the fuel economy to meet the stricter legislation, it is required to determine the AGS operating point to maximize the reduction on aerodynamic drag without jeopardizing the AC performance. Another side effect of AGS is related to engine part thermal damage and over-heating [7], but this part is beyond the scope of this work. The illustration for the front-end air flow with AGS open and close conditions is shown in Figure 1-3.
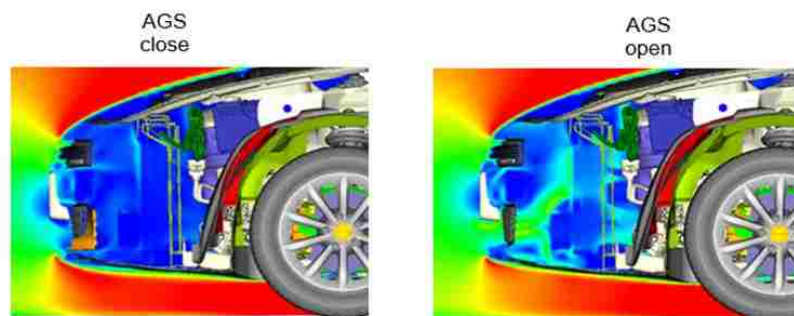
Figure 1-3: Illustration of front-end air with active grille shutter open vs close condition. While the AGS is open, the air flows through then complex engine compartment which increases drag but enhances the heat transfer for the engine cooling system and the AC system. When the AGS is fully closed, the air flows around the vehicle, which reduces drag but may weaken the cooling performance of the engine cooling system and the AC system. In this graph, the color represents the velocity of the airflow. Blue is the lowest while red is the highest.

1.3   Project outline

The thesis focuses on the impact of AGS on the compressor power consumption and the fuel economy. For this study, refrigerant loop model, cabin model and a driveline model are used. As shown in Figure 1-4, the compressor power consumption along with blower power is fed into the driveline model to predict the corresponding fuel consumption. The AC model and the cabin model are created and calibrated in AMESim by the author by adopting the method that was initially developed by Natarajan et al, 2013 [9]. The driveline simulations are run on an existing in-house model in AVL Cruise. The calibration process of the AC and cabin model includes tuning certain parameters in the models to match the specific simulation results with the corresponding experimental measurements. The simulation process includes both steady-state simulations and transient cycle simulations to study the effects of the AGS position on the AC compressor and the fuel consumption under different ambient conditions.
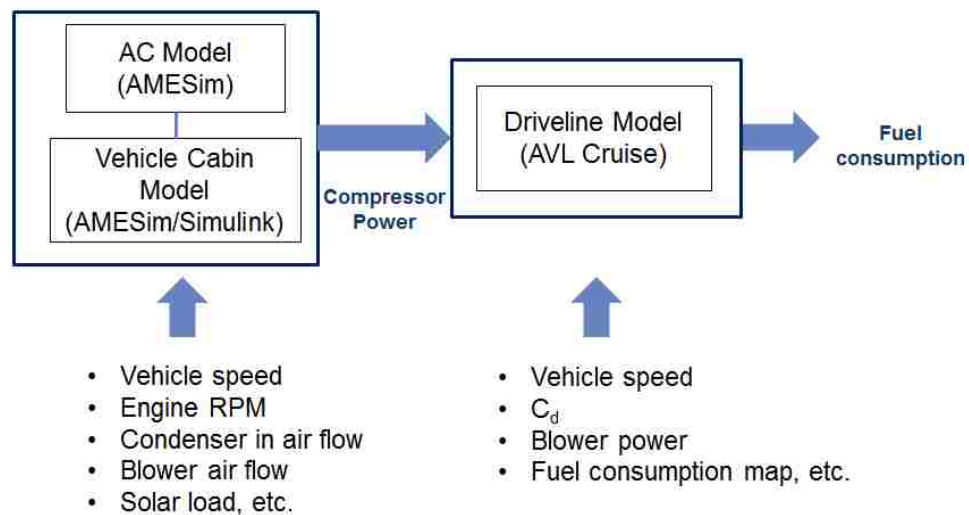
Figure 1-4: Simulation process of this thesis.

The study done in this thesis is carried out with Chrysler Pacifica 2017, it is a seven-seat minivan with dual evaporator AC system. The vehicle is equipped with a 3.6 L V6 engine.

The AGS on this vehicle is located in the highlighted area as shown in Figure 1-5. Behind the lower grille, there are the shutters which open and close according to the driving condition.

Figure 1-5: AGS is located in the lower grille as shown in the highlighted area [10].

Since the focus of the simulation is to investigate the influence of the AGS position on the fuel consumption, it is essential to calibrate the AC and cabin model so that the driveline model has the AC compressor power as an accurate input. The AC model and the cabin model are both calibrated with the cabin cool-down (CCD) test individually. Then the two models are connected to check if the integrated model has a good correlation with the experimental measurements. Since the AGS has an impact on the aerodynamic performance of the vehicle which varies with the vehicle speed [7], it is also interesting to see the results of the model simulated with drive cycles.

On the component level, it is informative to see the impact of the AGS position on the AC components performance which includes:

- Compressor power consumption
- Compression ratio
- Coefficient of performance

1.4   Major assumption

The major assumption for modeling the AC system, the cabin model in AMESim is as below.

- The temperature and the flow rate of the front-end air flow distributed on the condenser are assumed to be uniform for all the simulations. It is a reasonable assumption at high vehicle speed driving conditions.

In real condition, the air flow distributed on the condenser surface is not uniform especially at lower vehicle speed. However, the air flow rate increases as the vehicle speed increases, and it becomes very close to uniform distribution when the vehicle reaches highway speed. With this assumption, the simulated compressor power could be slightly smaller than the real case.

7

CHAPTER 2 LITERATURE REVIEW AND THEORY

2.1 Active grille shutter studies

Active grille shutter as a relatively new technology to improve fuel economy has been studied by many scholars in recent years. El-Sharkawy et al., 2011 [7] conducted a series of experimental tests to evaluate the effect of an active grille shutter on the AC performance. The tests were performed at highway speed and four different ambient conditions. Since the relationship between the aerodynamic power and the speed is expressed in equation (2-1), the aerodynamic power is proportional to velocity cubed. The aerodynamic benefit is more evident at higher speed. The vehicle speed during the test was maintained higher than 100 km/h. The power consumption by the cooling fans and the compressor were both considered to maximize the aerodynamic benefit. However, the actual improvement in fuel consumption was not quantified.

$$aerodynamic\ power = Cd \cdot A_{frontal} \cdot \frac{1}{2} \cdot \rho v^3 \qquad (2\text{-}1)$$

- Cd: coefficient of drag
- $A_{frontal}$: reference frontal area [m^2]
- ρ: density [kg/m^3]
- v: velocity [m/s]

Markowitz, 2011 [11] investigated into the aerodynamic benefit of the AGS on the vehicle energy consumption while considering the AC compressor power consumption by using an experimental method. His work optimized the amount of the AGS opening at a certain vehicle speed by balancing the aerodynamic benefit and the compressor power. He estimated the compressor power by using the compression ratio obtained from each test. The equation 2-2 is used to compute the compressor power, where x is the specific heat ratio.

$$Compressor\ power \sim \left(\frac{P_{disc}}{P_{suct}}\right)^{\frac{x-1}{x}} - 1 \qquad (2\text{-}2)$$

He stated that the COP increases as the AGS opening increases and the compressor power decreases as the opening increases. Also, more AGS opening is required at lower vehicle speeds. His work also concluded that at any case where the AGS is not fully open, the electric fan should not be running. The fan control would be more effective after the AGS is opened.

Pfeifer, 2014 [12] investigated the potential benefits of AGS application, which include aerodynamic drag reduction, shorten cold start phase and faster cabin heating, noise reduction in the engine bay and protection on the cooling system during extreme ambient condition. He introduced many AGS optimization methods in terms of geometric optimization for the shutter blades and so on. However, his work did not involve optimizing the AGS control strategy.

Bouilly et al., 2015 [13] utilized model-based simulations to evaluate the potential fuel economy benefit of the AGS by considering vehicle thermal management. They stated that a model-based development method could evaluate a new technology before the prototype testing. An integrated model was built and validated in AMESim against fuel consumption, coolant temperature and oil temperature. The control strategy was designed by considering fuel consumption, coolant temperature difference, and the total AGS flap angular displacement. Experimental tests were conducted to validate the accuracy of the model. To obtain the actual fuel consumption, CO_2 were measured during the tests. Their work suggested that a five-step actuation of both upper and lower AGS moving simultaneously was the best solution and increasing the intermediate steps above five did not bring more benefit. However, from an economic point of view, the cost versus benefit should be considered. Their work provided a methodology to utilize 1D simulation software to determine the AGS control strategy on a transient cycle. Their work focused on the fuel economy benefit of the AGS while considering the performance of the engine cooling system, they did not consider the impact of the AGS position on the AC system.

Cho et al., 2017 [14] reported an optimized AGS control strategy on a highway drive cycle to improve fuel economy and underhood cooling performance. The SUV vehicle model was built in powerFLOW which is CFD simulation software to solve fluid flow design problems. The fuel consumption was predicted by another model where the engine power is calculated by considering all the drive cycle loads. Finally, the fuel consumption and radiator heat rejection were compared with AGS fully open condition. Their work reported improvement in the fuel economy while maintaining the engine cooling requirement of 1.3% to 1.5% depending on the ambient temperature.

The above studies all investigated into the AGS optimization process. Most of these did not consider the impact on the AC system power consumption which is one of the largest auxiliary loads while operating in a vehicle. In this thesis, a model-based method is developed to quantify the potential fuel economy improvement due to AGS technology during the early design stage of the vehicle. It considers the tradeoff between the aerodynamic power and the AC system power consumption focusing on the AC system cooling performance.

CHAPTER 3 AC SYSTEM MODELING AND AGS VERSUS COMPRESSOR POWER STUDY

3.1 Simulation software

In the present thesis, a system simulation approach is used to model the refrigerant loop, vehicle cabin and their interaction. It is important to study the transient behavior of the vehicle in different scenarios especially when introducing a new technology to the vehicle. This step helps to understand the impact of the AGS on specific AC performance parameters under various driving conditions. The software must be able to run transient simulations and most importantly, it requires the inclusion of solid material properties and two-phase material modeling for building a complete AC system and a cabin thermal model.

AMESim is the software used to create the AC system and the cabin model in this section. It is commercial software that is widely used in the automotive industry. This 1D simulation platform simplifies multi-domain integration and accurately predicts multi-disciplinary system performance [15]. It has numerous libraries which provide predefined components from different physical domains such as fluid, thermal, mechanical, etc. More importantly, specific two-phase flow properties and material properties can be found in the library, which is crucial for building the air conditioning system and the cabin model.
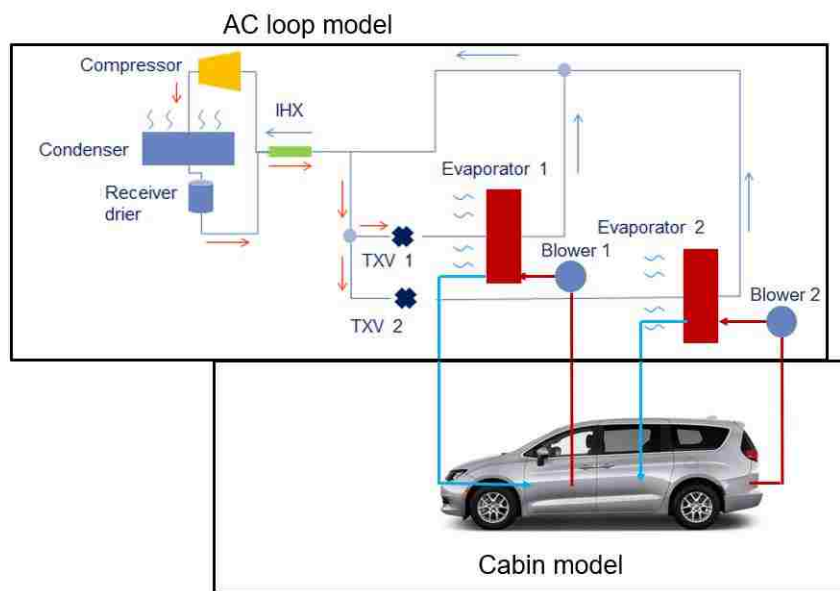
Figure 3-1: Illustration of the AC loop model which contains all the major components in the AC system and how the AC loop is integrated with the cabin model.

3.2   Model components

This section gives a brief introduction to the major components of the AC system. As shown in Figure 3-1, the AC system has two evaporators, one at the front of the cabin and one at the rear. So accordingly, there are two TXVs and two blowers. All the components that are described in this section are modeled and calibrated within AMESim. R1234yf is the refrigerant used for the AC system. There are pre-developed models inside AMESim that can be used directly to simulate these components. They require user-defined parameters and proper calibration process to function correctly. For more detailed modeling process, please see APPENDIX B.

3.2.1   Compressor

The AC system of the Pacifica 2017 is equipped with a variable displacement compressor (VDC) with an external regulator. For reference, the cross-section of a swash plate type of variable displacement compressor is shown in Figure 3-2. The main components are labeled in the figure. The control mechanism functions in a way that as the AC load decreases, the regulator senses that there is a difference between the evaporator outlet temperature with the target temperature, the swash plate is adjusted by the actuator to a steeper angle, and the stroke of the piston deceases accordingly. Similarly, the stroke of the piston increases as the AC load increases.

The compressor model in AMESim uses efficiency maps as functions of compressor speed and pressure ratio to predict the flow rate, enthalpy increase and torque. The volumetric efficiency and the isentropic efficiency as functions of compressor rotary speed and pressure ratio are given by the supplier. Although the mechanical efficiency also changes as the compressor rotates at different speeds, due to lack of experimental information, the mechanical efficiency is assumed as a constant for all the simulation. Since the compressor is coupled with the engine, the compressor speed is proportional to the engine speed. Based on these performance maps, the model can calculate the mass flow rate, enthalpy increase, and the compressor torque.

The volumetric efficiency (η_v) is used to calculate the mass flow rate of the refrigerant at compressor outlet:

$$\dot{m}_{comp-out} = \eta_v \cdot \rho_{suct} \cdot N \cdot S$$

$(3\text{-}1)$

The isentropic efficiency (η_{is}) is used to calculate the enthalpy increase across the compressor:

$$\Delta h = h_{disc} - h_{suct} = \frac{h_{disc-is} - h_{suct}}{\eta_{is}}$$ (3-2)

Where:

- h_{disc}: actual discharge specific enthalpy [kJ/kg]
- $h_{disc-is}$: isentropic discharge enthalpy [kJ/kg]
- h_{suct}: suction specific enthalpy [kJ/kg]

And the mechanical efficiency (η_{mech}) is used to calculate the compressor torque as follow:

$$T = \frac{\dot{m}_{ref} \cdot \Delta h}{\eta_{mech} \cdot N}$$ (3-3)
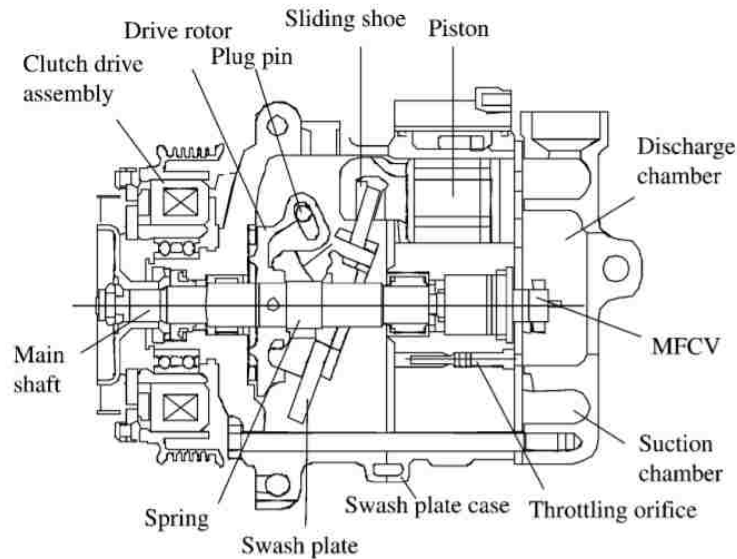
Figure 3-2: Swash plate variable displacement compressor [16].

3.2.2 Condenser and evaporator

The condenser and evaporator both serve as heat exchangers inside the AC system. The condenser releases heat from the refrigerant to the ambient and the evaporator absorbs heat from the surroundings. The AC system is equipped with a parallel flow tube and fin condenser, a plate, and fin front evaporator and a tube and fin rear evaporator. The condenser has four passes. An example of the four-pass parallel flow condenser is shown in Figure 3-3. The figure shows the

cross-section of a condenser. The first pass is de-superheating pass, followed by cooling and sub-cooling regions. The front and rear evaporators have different geometries and orientations. The evaporator models can be constructed in AMESim by using different pre-defined sub-models which represent the corresponding geometric shape and orientation. All the heat exchanger models must consider the internal convective heat transfer, the conductive heat transfer in the condenser walls and the external heat transfer between the wall and the air [17]. The equations below define the internal and external convective heat transfer:

$$\dot{Q}_{int} = h_{int} \cdot A_{int} \cdot (T_{ref} - T_{wall}) \qquad (3\text{-}4)$$

$$\dot{Q}_{ext} = h_{ext} \cdot A_{ext} \cdot (T_{air} - T_{wall}) \qquad (3\text{-}5)$$

$$h = Nu \times \frac{\lambda}{D_h} \qquad (3\text{-}6)$$

Where λ is the thermal conductivity in W/ (K·m), D_h is the hydraulic diameter of the tube. And the wall temperature is calculated as follow:

$$\frac{dT_{wall}}{dt} = \frac{\dot{Q}_{int} + \dot{Q}_{ext}}{m \cdot c_p} \qquad (3\text{-}7)$$

The calibration process of the heat exchanger models involves using the optimization tool in AMESim to find the optimum values of the tuning parameters that best match experimental data regarding to heat reject and pressure drop. The experimental data of the heat exchangers that is provided by the supplier is the calorimeter data with heat rejection values for a range of refrigerant side and air side conditions. After calibrating the heat exchangers, they should mimic the calorimeter behavior. So, to calculate the heat exchange between the solid part and the ambient air, the geometry details of the heat exchanger and the external heat transfer coefficient are critical. In AMESim, the heat transfer coefficient is calculated according to the Nusselt correlation, and the relationship between the Nusselt number and the external flow is given by:

$$\text{Laminar regime: } Nu = constant \qquad (3\text{-}8)$$

$$\text{Turbulence regime: } Nu = a \cdot Re^b Pr^c \qquad (3\text{-}9)$$

For the laminar regime, the Nusselt number is a constant, and it depends on the geometry of the heat exchanger. For turbulent regime, the Nusselt number is a function of the Reynolds number and the Prandtl number. In the equation 3-9, the coefficient c is assumed as a constant of 0.4 for cooling cases [17], the coefficient a and b are used as tuning parameters to tweak the value of the Nusselt number and hence the external heat transfer coefficient to mimic the supplier given performance. As the external heat exchange is adjusted, the heat rejection performance of the heat exchange also changes along. Also, the external heat exchange is a function of the wall temperature which depends on the internal heat exchange, and the internal heat exchange is calculated according to the flow condition and the correlations that are pre-defined in AMESim. The internal heat exchange can also be adjusted by modifying a parameter called 'refrigerant side heat transfer gain'. Similarly, the pressure drop can be tweaked by modifying the 'pressure drop gain' parameter. At the end, the model should predict the heat rejection and the pressure drop accurately.
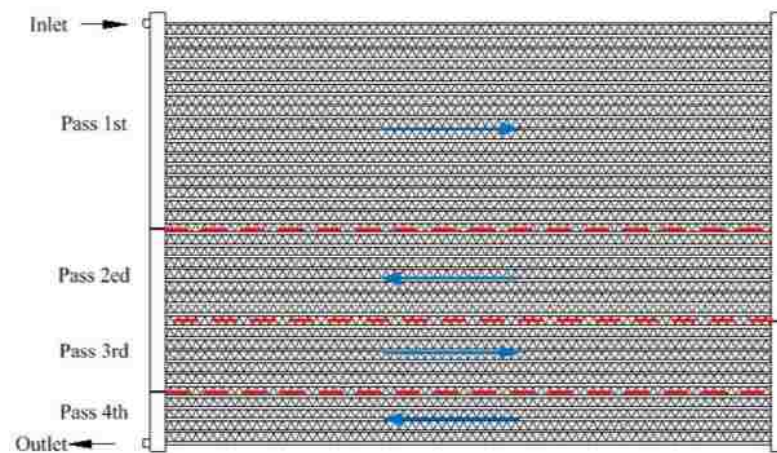
Figure 3-3: Multi-pass parallel flow condenser [18].

3.2.3   Thermal expansion valve

The thermal expansion valve serves as a flow metering device. It controls the mass flow rate of the refrigerant according to the superheat at the evaporator outlet. This function is achieved by a diaphragm that controls the opening of the pin valve which regulates the refrigerant. Three pressures are acting on the diaphragm in a TXV. The refrigerant within the evaporator applies pressure under the diaphragm; the spring pressure applies pressure to the pin valve which also applies pressure under the diaphragm; pressure from the temperature sensing bulb acts above the

diaphragm. The return spring exerts resistance against the pin valve movement can be calibrated to adjust the amount of the valve lift. Usually, the valve lift changes when the cooling load changes, it is important to have the accurate valve lift in the simulation because it determines the refrigerant mass flow rate under different conditions. The temperature sensing bulb in the TXV is connected to the evaporator outlet, and it is filled with an inert fluid which is different from the refrigerant. When a higher cooling load is demanded, the temperature at the evaporator outlet will increase. Due to the increased temperature, the pressure inside the bulb increases because of the internal fluid expansion. This pressure increment is transferred via a capillary tube to the top of the diaphragm and enables the diaphragm to overcome the other two pressures that are acting under the diaphragm, the valve opens further and lets more refrigerant to flow through the evaporator to provide a higher cooling rate. On the contrary, if the cooling load decreases, the temperature at the evaporator exit will decrease. The pressure acting on top of the diaphragm decreases accordingly and become less than the pressure acting under the diaphragm. As a result, the diaphragm moves upward and reduces the valve opening and thus lowers mass flow rate of the refrigerant [4].

The calibration of TXV model requires a four-quadrant diagram that is provided by the supplier. The first three quadrants are the evaporator pressure as a function of thermal sensing bulb fluid; the evaporator outlet pressure as a function of valve lift; the mass flow rate as a function of the valve lift. The fourth quadrant is the reference mass flow rate as a function of the evaporator outlet temperature. The first three curves are inputs and the TXV model is calibrated to match the final curve against the supplier data. The cross-section of a typical thermal expansion valve is shown in Figure 3-4.

3.2.4   Internal heat exchanger

The internal heat exchanger (IHX) has a double-pipe configuration, it allows the internal flow in the tubes to exchange heat with one another through an aluminum medium. The hot liquid refrigerant from the condenser flows through the inside tube, and the external tube is filled with cool refrigerant vapor that is flowing out of the evaporator. The refrigerant at the condenser exit is sub-cooled, but the IHX transfers even more heat out of the liquid refrigerant and sub-cools it further. This improves the cooling efficiency since the liquid refrigerant can absorb more heat while it passes through the evaporator. Literature indicated that the improvement in the cooling capacity of the R1234yf AC system with the IHX increased up to 7% [20]. The 'gained' cooling capacity can also be used by the engineers to downsize the compressor, which reduces the weight

of the AC system and the load on the engine. Figure 3-5 demonstrates a simplified double-pipe IHX and its cross-section.

The IHX can be viewed as a heat exchanger with an inner and an outer chamber; the model can be built in AMESim with the two-phase flow pipe sub-models and a thermal mass sub-model which represents the aluminum medium between the two streams of flow. For calibration, the pressure drops in each tube and the heat transfer calculated from the model are compared with the experimental data. The model is calibrated against the performance data that is provided by the supplier. By assigning the corresponding boundary conditions, the model can calculate the heat transfer rate and the pressure drop which will be comparable with the test results.
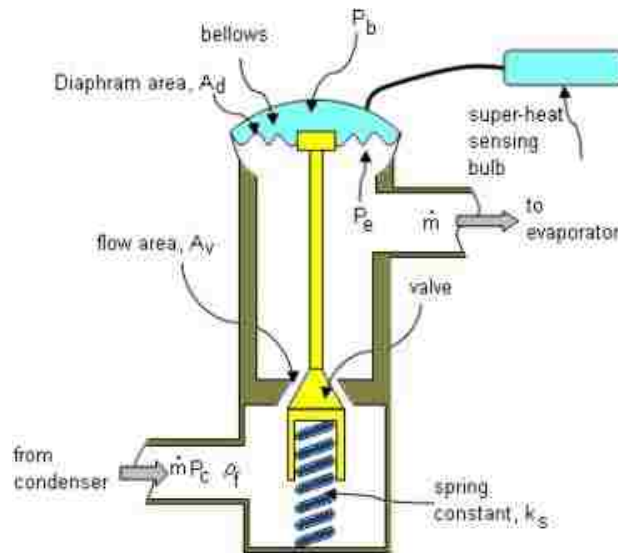
Figure 3-4: The cross-section of a typical thermal expansion valve with important components labeled [19].
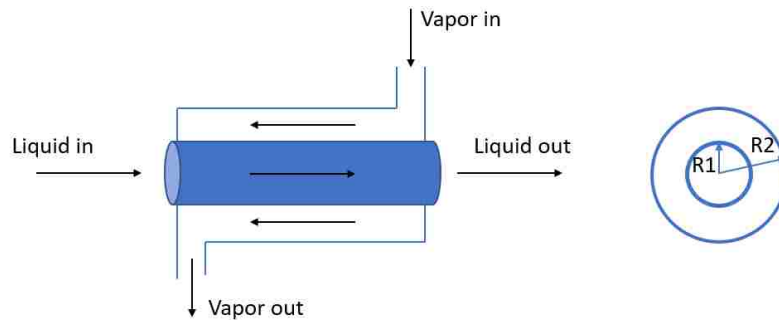
Figure 3-5: An example of a double tube type of internal heat exchanger with the cross-section showing on the right.

3.3   Vehicle cabin model

The vehicle cabin model is essential when the AC is running in recirculation mode. The cabin model provides the continually changing air properties to the evaporator inlet as inputs and the properties of the air coming out of the evaporator serves as inputs to the cabin model and form a complete loop. The model is constructed by dividing the cabin into several sub-components (door, roof, windows and so on). The thermal interactions between each sub-component and the cabin air are considered. The model is built based on these energy transfer paths. After that, the geometric information, material properties, and boundary conditions are defined in the model. Finally, the model is calibrated against the cabin cool-down test (CCD) to ensure that the model has the same thermal behavior as the actual vehicle. This calibration process involves adjusting the internal heat transfer coefficients between the internal surfaces and the cabin air to minimize the error between simulation results and tests. A built-in optimization tool is able to optimize the values of the tuning factors and minimize the total error between the simulation result and the test data along the cycle. After calibration, the model is connected with the AC loop model to predict the cabin air temperature and most importantly, the compressor power consumption under different ambient conditions. The integrated model in AMESim is shown in Figure 3-6.

3.4   Driveline model

The in-house driveline model was developed and calibrated in AVL Cruise. The model was calibrated against various transient cycles to ensure the accuracy for predicting fuel consumption.

The driveline model can predict the engine speed, gear selection, and fuel consumption according to the user-defined road profile and auxiliary load. The blower and compressor power consumption are input into the driveline model as auxiliary loads. Other inputs such as the coefficient of drag and the frontal area are used to calculate the aerodynamic drag. Each simulation is running with AGS open and then AGS closed to calculate the corresponding fuel consumption.

17
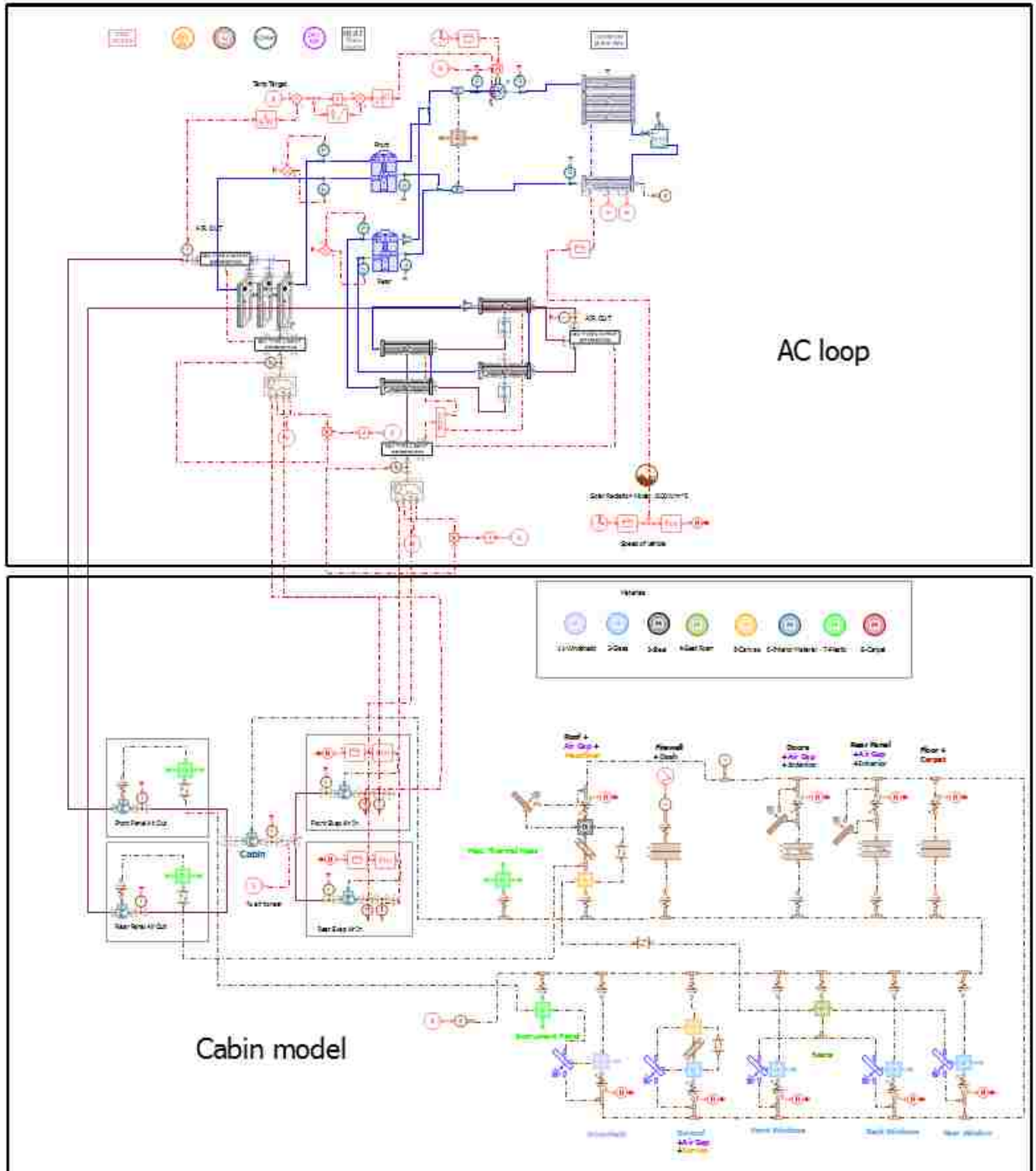
Figure 3-6: The integrated AC loop and cabin model in AMESim.

3.5 Simulation plan

3.5.1 Steady-state simulation

The first part of the simulation is done in AMESim environment. The goal is to study the effect of the front-end air flow and the blower settings on the compressor power consumption. The steady-state simulations are carried out in fresh mode which means that the air flows into the evaporator is the ambient air, and the effect of the cabin thermal behavior on the AC system is excluded. A parametric study is done to evaluate the impact on compressor power of ambient temperature, blower setting, and AGS position. Under different boundary conditions, the compressor power and the fuel consumption vary. Two mid-ambient temperatures, 26.7°C and 32.2°C, are selected as the real-world conditions to investigate the impact of ambient temperatures on the compressor power. The blowers have seven settings in total, Lo, M1, M2, M3, M4, M5 and Hi range from the lowest to the highest blower power. For simplicity, the front and rear blowers are set at the same modes during the simulation: the low mode, the high mode, and the intermediate mode M3. Also, since the improvement on the aerodynamic performance of a vehicle is significant only at highway speed, the vehicle speed is set at 105 km/h (65 mph) for the steady-state simulation. Since the AGS position affects the compressor by changing the condenser inlet air flow, the model input that represents the AGS position is the condenser inlet air flow rate. The corresponding air flow rate would be higher with AGS open and lower with AGS closed. The relative humidity is set at 19% to be coherent with the CCD test that is used for calibration in this thesis and HVAC system design in the industry. However, the relative humidity in real life during summer can be much higher than 19%. Higher relative humidity will result in higher load on the AC, which means the AC must consume more energy to achieve the same cooling performance. The effect of altitude is not included in this study; it is set at zero meters above the sea level. In real life, if the altitude is higher, it is expected to have a higher compressor power due to the less dense air. The simulation plan and the boundary conditions are listed in Table 3-1.

The objective of these simulations is to compare the compressor performance under AGS open and AGS close conditions. The second part is to calculate the fuel consumption of each case in the AVL driveline model. By comparing the fuel consumption under different boundary conditions, the AGS position can be justified to have better fuel economy.

Table 3-1: Boundary conditions of the steady-state simulations.

No.	Ambient temperature	Ambient air relative humidity	AGS position	Condenser inlet air flow rate	Blower setting	Front blower air flow rate	Rear blower air flow rate
	°C	%		CFM		CFM	CFM
1	26.7	19	Open	CFM_{open}	Lo	CFM_{F_Lo}	CFM_{R_Lo}
2	26.7	19	Open	CFM_{open}	M3	CFM_{F_M3}	CFM_{R_M3}
3	26.7	19	Open	CFM_{open}	Hi	CFM_{F_Hi}	CFM_{R_Hi}
4	26.7	19	Close	CFM_{closed}	Lo	CFM_{F_Lo}	CFM_{R_Lo}
5	26.7	19	Close	CFM_{closed}	M3	CFM_{F_M3}	CFM_{R_M3}
6	26.7	19	Close	CFM_{closed}	Hi	CFM_{F_Hi}	CFM_{R_Hi}
7	32.2	19	Open	CFM_{open}	Lo	CFM_{F_Lo}	CFM_{R_Lo}
8	32.2	19	Open	CFM_{open}	M3	CFM_{F_M3}	CFM_{R_M3}
9	32.2	19	Open	CFM_{open}	Hi	CFM_{F_Hi}	CFM_{R_Hi}
10	32.2	19	Close	CFM_{closed}	Lo	CFM_{F_Lo}	CFM_{R_Lo}
11	32.2	19	Close	CFM_{closed}	M3	CFM_{F_M3}	CFM_{R_M3}
12	32.2	19	Close	CFM_{closed}	Hi	CFM_{F_Hi}	CFM_{R_Hi}

3.5.2 Transient cycle simulation

The transient simulation plan involves two drive cycles at 26.7°C and 32.2°C. These tests are intended to optimize thermal system during real-world driving conditions in support of improving fuel economy. The velocity map of this cycle is shown in Figure 3-7. The vehicle speed increases from 48 km/h to 129 km/h with each speed segment lasts for 900 s. This cycle is suitable for the investigation in the present thesis since it covers both city speed and highway speed, and the actual tests measure the fuel consumption with AC on, which are the very few tests that focus on fuel consumption but also consider the performance of the AC system. Moreover, these transient cycle simulations can show how the variable displacement compressor responses when a sudden change in the condenser air flow occur. The performance of the variable displacement compressor can be investigated based on the simulation results.
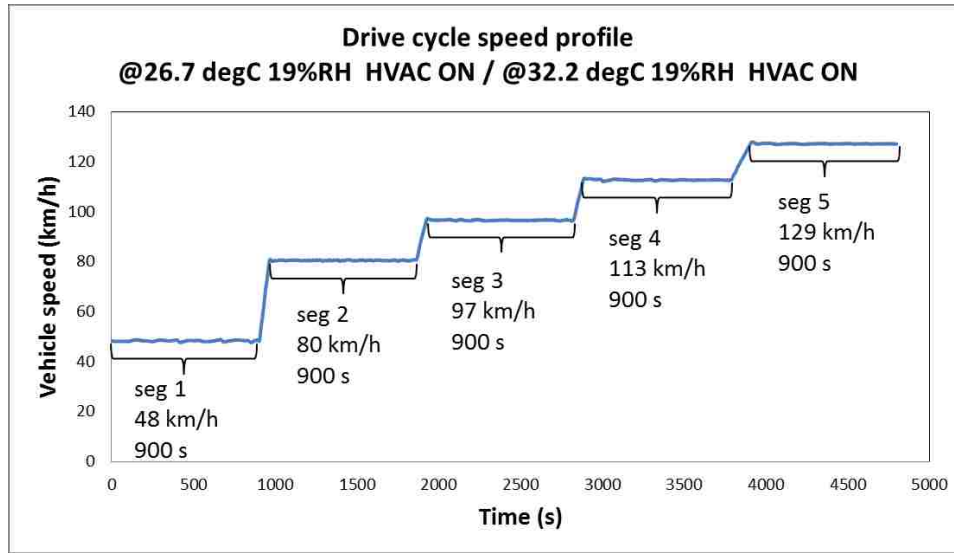
Figure 3-7: The vehicle velocity map of the drive cycle for the transient simulation.

Table 3-2: Ambient condition of the drive cycle at 26.7 ℃ and 32.2 ℃.

Parameters		
Ambient temperature	26.7°C	32.2°C
Relative humidity	19%	19%
Solar load	None	None

Similarly, the second part involves computing the fuel consumption in the driveline model. It will show clearly how the AGS benefits the fuel consumption in different speed segment. The coefficient of drag is the key input of the driveline model. It enables the model to justify the aerodynamic improvement when the AGS is in closed position. The potential benefit due to the AGS technology is further explained by calculating the reduced fuel consumption by comparing the vehicle driving for a four-hour trip with AGS fully open and fully close. The vehicle is assumed to travel at a constant speed of 105 km/h.

CHAPTER 4 RESULTS AND DISCUSSION

4.1 AC and cabin model calibration in AMESim

The sub-components in the AC model are calibrated against the supplier provided performance data. The details can be found in APPENDIX B.

The cabin model is calibrated against the CCD test. The calibration process involves minimizing the difference between the simulation results and experimental test. The calibrated cabin model is then integrated with the AC model and the integrated model is validated against two more cool-down cycles to ensure the errors for the simulated cabin temperature, compressor suction and discharge pressures and the compressor power are within acceptable ranges.

Most of the vehicle cabin information is obtained from the CAD data, the material properties are assumed from literature and some are provided by the supplier. However, the convective heat transfer coefficients inside the cabin are undefined. Usually, these parameters are defined experimentally due to the complex geometry of the vehicle cabin. In this model, these heat transfer coefficients are used as tuning factors to match the simulated cabin thermal behavior with the experimental test data. Also, since we cannot capture all the thermal mass inside the cabin, the miscellaneous mass is used to approximate what is left out. Theoretically, the more heat transfer coefficients used to calibrate the model, the more accurate the model will be. Because the heat transfer coefficient of each surface is different due to the different geometry and air flow condition, it does not make sense to assume that the heat transfer coefficients for all the windows are the same. However, the process for calibrating the model with too many factors will consume a significant amount of time. Six parameters were used to calibrate the model to compromise between the accuracy and the time-consuming. The higher and lower limits of the parameters are set in advance to make sure that the values of the parameters are reasonable. The parameters and their final values are shown in Table 4-1. These parameters are tuned to minimize the total error along the cycle between the simulated cabin air temperatures and panel temperatures and the test data. The definition of the cost function is shown in equation 4-3. After that, other parameters such as the compressor power and the compressor pressure are checked. If the simulation result does not match the experimental test, the calibration process must be repeated by narrowing or expanding the upper and lower limit of the tuning parameters.

Figure 4-1 shows the comparison between the test data and the calibration result. The values are normalized by dividing the data point by the largest value among that set of data. It is crucial to

ensure that the prediction for compressor power consumption is accurate. The relative error for the average cabin temperature, compressor suction and discharge pressure and the compressor power consumption are 3.1%, 6.3%, 3.8% and 8.4%. The definition of the relative error is shown in equation 4-1 and equation 4-2, where n is the number of samples, y_{ref} is the target value while y_{sim} is the simulation result. The model is checked with another two cycles; the results are included in APPENDIX E. At this point, the model is well calibrated and ready for the simulations.

Table 4-1: The tuning parameters used in the Amesim cabin model to match the simulation results with the experimental tests.

Parameter	Notation	Value
Convective heat transfer coefficient of the doors	ℏ_1	70.2 W/(m²K)
Convection coefficient of the windows	ℏ_2	7.8 W/(m²K)
Convective heat transfer coefficient of the floor	ℏ_3	1.61 W/(m²K)
Convective heat transfer coefficient of the roof	ℏ_roof	2.6 W/(m²K)
Miscellaneous mass	M_misc	10 kg
Convective heat transfer coefficient of the miscellaneous mass	ℏ_misc	127.7 W/(m²K)

$$e(t) = y_{ref}(t) - y_{sim}(t) \qquad (4\text{-}1)$$

$$err_{average} = \frac{1}{n}\sum_{t=0}^{t_n}\left|\frac{e(t)}{y_{ref(t)}}\right| \qquad (4\text{-}2)$$

$$F(x) = \sum_{t=0}^{t_n} e(t)^2 \qquad (4\text{-}3)$$

Calibration results against the cabin cool down test
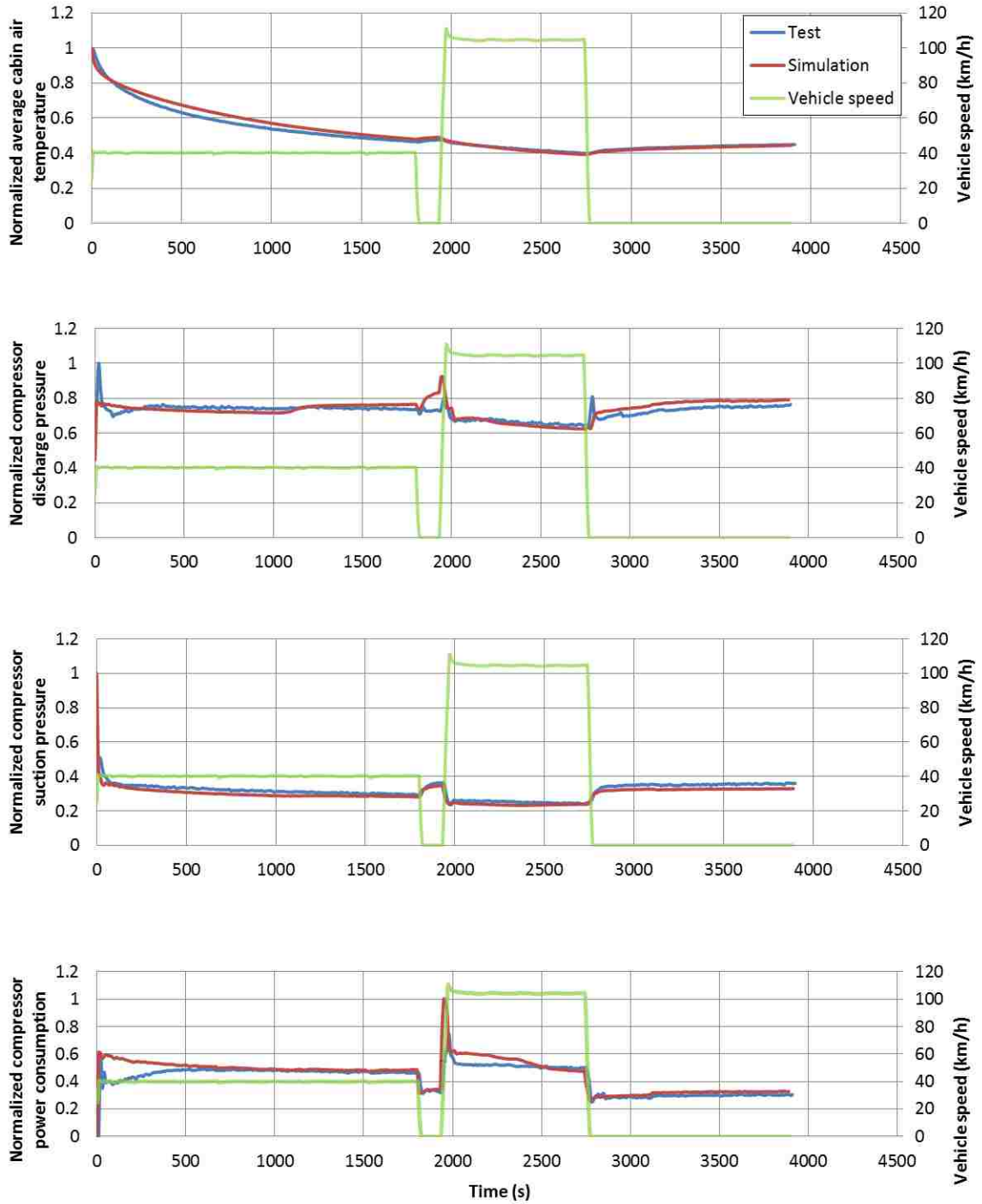
Figure 4-1: Calibration results for AC and cabin model against the CCD test. The figures include the comparison between the simulation and test date of the average cabin temperature, compressor discharge and suction pressure and the compressor power consumption. The values are normalized by dividing the data point by the maximum value among that set of data.

4.2 Steady-state simulation

This section shows the results of the steady-state simulation under 100% fresh mode. Only the stand-alone AC loop model is used for the simulations. The simulation time for each run is 5 minutes to reach a steady-state condition. The following subsections will study the impact of different parameters on the compressor power consumption from the steady-state simulation results.

4.2.1 Compressor power consumption

The results for the steady-state simulation in AMESim at 26.7°C and 32.2°C are shown in Figure 4-3 and Figure 4-4.

The values are normalized according to the equation 4-4, where y_{min} is the smallest value among the data points while y_{max} is the largest value. By comparing the AGS open with AGS close results, the compressor generally consumes more power when the AGS is closed due to insufficient incoming air flow.

$$y_{normalized} = \frac{y(t) - y_{min}}{y_{max} - y_{min}} \qquad (4\text{-}4)$$

Under the same ambient temperature, the AGS open and AGS close conditions are compared. The power consumption increases as the blower setting increases from low to high mode. As the blower setting increases, it brings more air flowing through the evaporator and increases the temperature of the refrigerant; the TXV senses the temperature rise and lifts the pin valve accordingly. The refrigerant flow rate increases and hence the compressor requires more power to compress more refrigerant. The compressor power also increases as the ambient temperature increases. As the ambient temperature increases, the heat rejected by the condenser from the refrigerant to the ambient air decreases. So, the compressor must work extra hard to rise the temperature of the refrigerant to promote heat exchange in the condenser to maintain the same cooling performance.

To investigate how much compressor power increases when the AGS is switched from open to close position, the delta compressor power consumptions by comparing AGS closed with AGS open condition are plotted in Figure 4-3 and Figure 4-4. The results show under both ambient conditions, the compressor power difference is the largest when the blower is set at high mode. On the contrary, the difference is tiny when the blower setting is low. Since at the Lo mode, the load on the AC is low, so the compressor power consumption is relatively low. If the AGS is

switched to closed position, the air flow rate decreases but it is still enough for the AC to meet the low cooling demand. So, the effect on the compressor power by closing the AGS is smaller with lower cooling load. The trend of the delta compressor power at 32.2°C is slightly different from the result at 26.7°C. The delta compressor power at 32.2°C with Lo and M3 blower modes is higher than that at 26.7°C. However, the delta compressor power at Hi mode is lower than the result at 26.7°C. This could be a result of the complex interaction between the sub-components in the AC system. Therefore, the impact of the ambient temperature on the delta compressor power cannot be concluded when the AC is running under fresh mode. However, the delta compressor power increases as the cooling load increases at 32.2°C, which is coherent with the results at 26.7°C.

4.2.2   Tradeoff between the AC compressor power and the aerodynamic power

Since the aerodynamic power is proportional to velocity cubed, the aerodynamic benefit will become significant at higher speeds. Figure 4-2 shows the reduction in aerodynamic power at different vehicle speed, it is calculated according equation 2-1. With this vehicle, the reduction in aerodynamic drag coefficient is 2% with AGS closed by comparing to with AGS open, and the reduction in aerodynamic power is 258 W at 105 km/h. By considering the tradeoff between the AC power consumption and the aerodynamic power, if the AC power consumption is more significant than the aerodynamic benefit, the AGS should remain open.
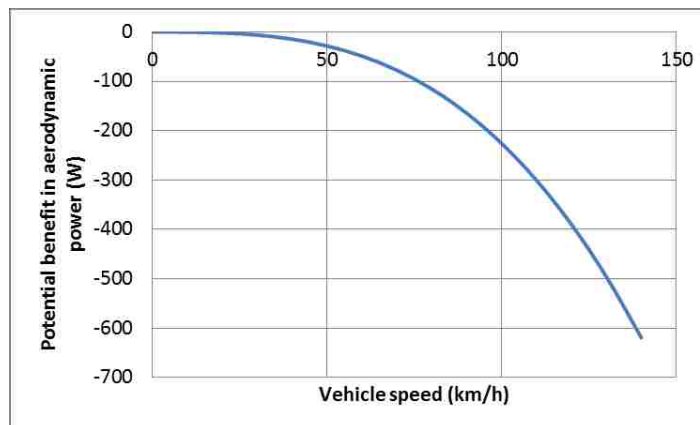
Figure 4-2: Potential aerodynamic benefits at different vehicle speed. It is the difference in aerodynamic power with AGS closed and AGS open.

Since the delta compressor power is much smaller than the reduction in aerodynamic power when the AGS is closed (258 W), the AGS should remain closed even with the highest AC load condition. This will be further verified by calculating the fuel consumption for both AGS open and close conditions.

Steady-state simulation results at 26.7°C
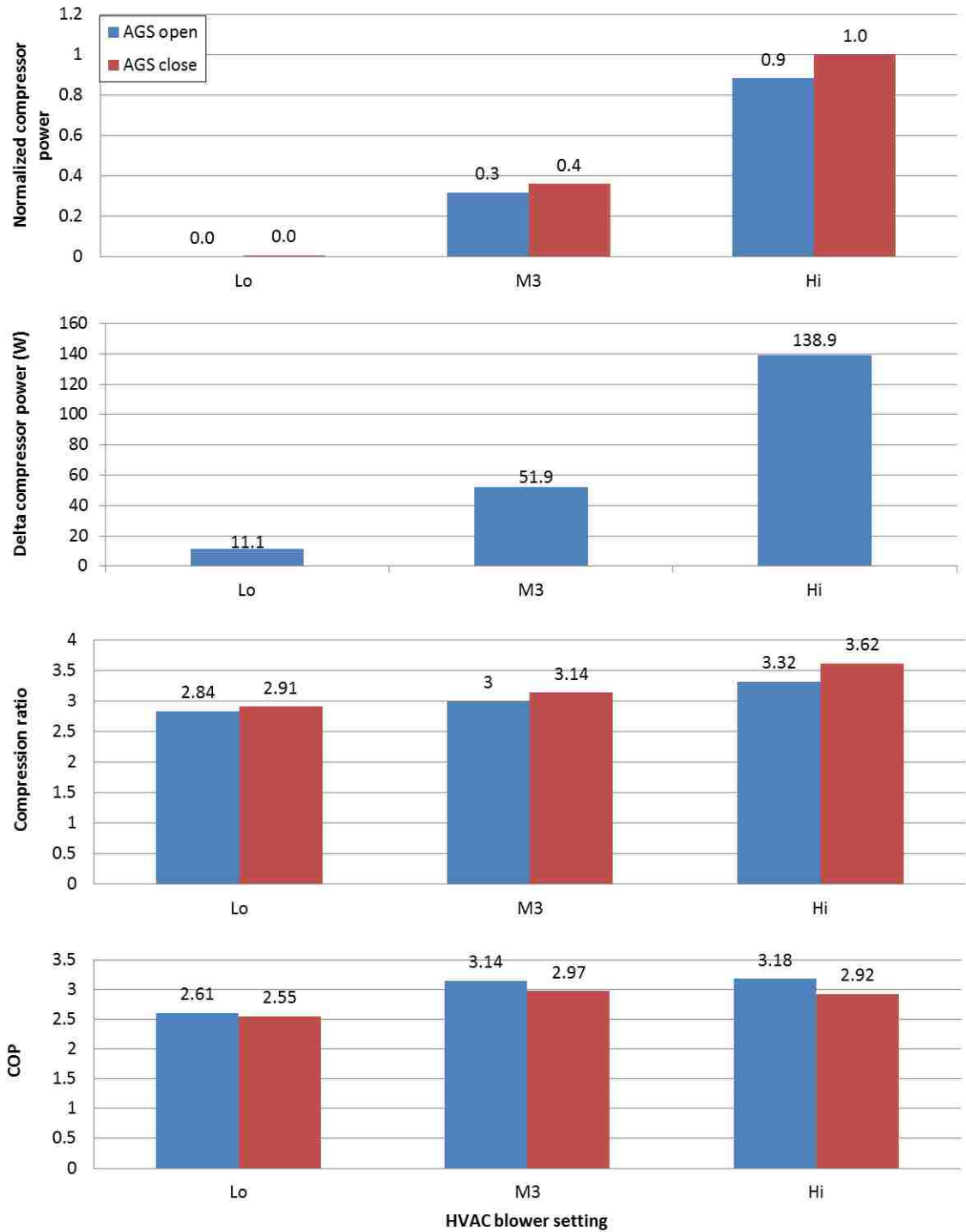
Figure 4-3: Steady-state simulation results at 26.7°C. The first figure shows the compressor power, the values are normalized according to equation 4-4. The second figure shows the delta compressor power by comparing AGS closed with AGS open condition. The third figure shows the compression ratio and followed with the coefficient of performance (COP).

Steady-state simulation results at 32.2°C
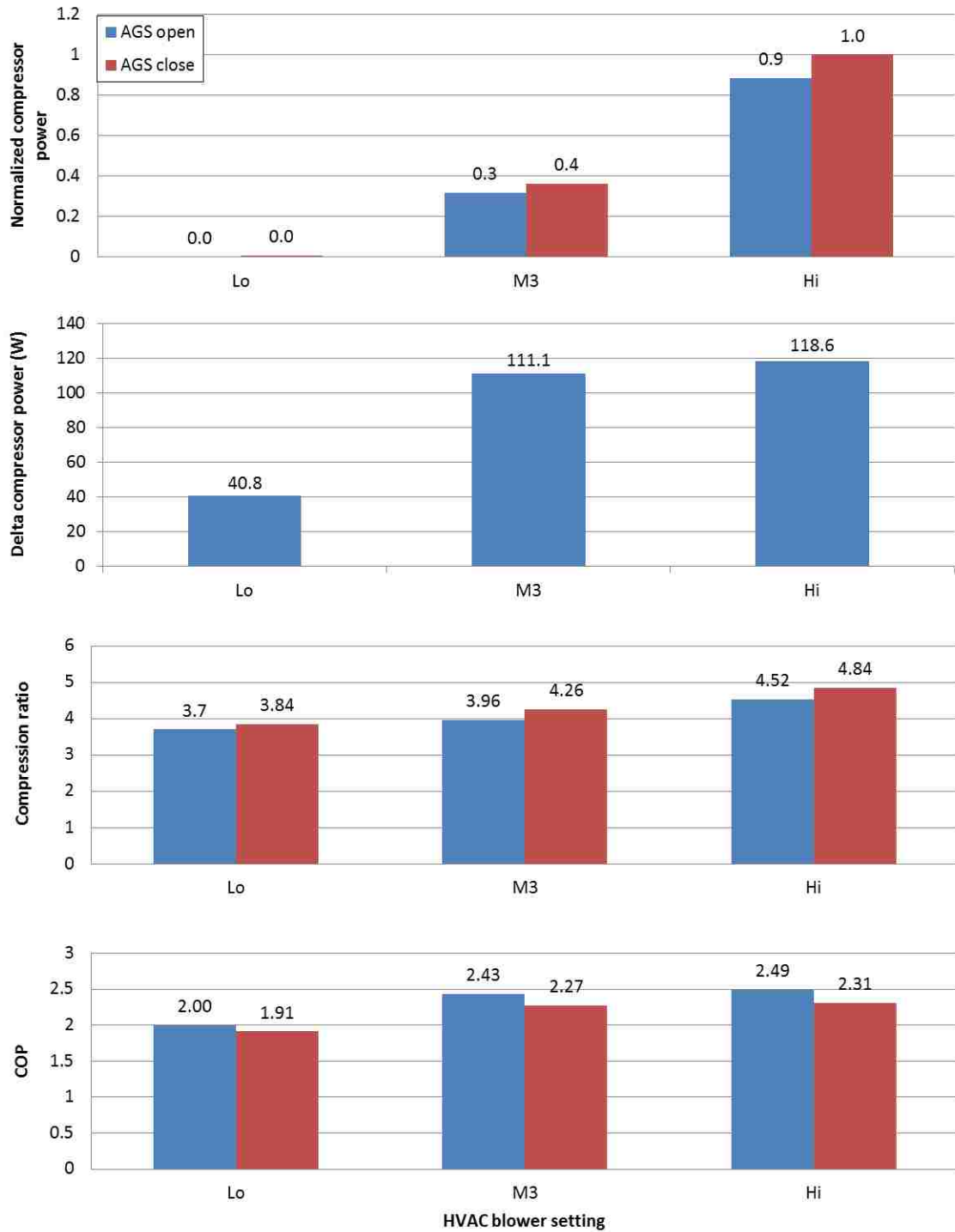
Figure 4-4: Steady-state simulation results at 32.2 °C. The first figure shows the compressor power, the values are normalized according to equation 4-4. The second figure shows the delta compressor power by comparing AGS closed with AGS open condition. The third figure shows the compression ratio and followed with the coefficient of performance (COP).

4.2.3 Impact of front end air flow on the AC performance

It is known that the compressor power consumption is proportional to the indexed compression ratio which is known as the ratio between discharge pressure and suction pressure [11]. As discharge pressure increases, the power consumption increases as the compression ratio increases. The results in Figure 4-3 and Figure 4-4 show that under the same road load, ambient condition and the same AGS position, the compression ratio increases as blower setting increases. Therefore, the compression ratio increases as the AC load increases. By comparing the AGS open with the AGS closed case, the compression ratio is higher with AGS closed, which means the compression ratio increases as the condenser inlet air flow decreases. Now, to compare the two sets of simulation with different ambient temperatures, it is evident that the compression ratio increases as the ambient temperature increases for both AGS open and closed conditions. Since the evaporator inlet air flow rate depends on the occupants need, the ambient temperature cannot be adjusted if the vehicle speed is constant, the only way to reduce the compressor discharge pressure is to increase the condenser inlet air flow. This can be achieved by adding an electric fan. However, whether the energy saved by the compressor compensates the energy used by the fan must be justified. Also, according to Markowitz, 2011 [11], the fan should not run while the AGS is not fully open. The best way to achieve enough air flow is to open the AGS, if the air flow is still insufficient, the fan should be triggered to lower the compressor discharge pressure and hence the compression ratio.

Another important parameter to evaluate the performance of the AC system is the coefficient of performance (COP). COP is the ratio between the evaporator cooling capacity and the compressor power consumption. Higher COP is always preferred for an AC system since it means more cooling power can be obtained by consuming the same amount of mechanical power in the system. The results indicate that the value of COP is generally larger than one. The COP of the AC system with AGS open is larger than that with AGS closed condition. This is because with AGS closed, the compressor needs more power to rise the temperature of the refrigerant to increase the heat rejected by the condenser. While the cooling load on the evaporator is the same as before, so the heat absorbed from the refrigerated area by the evaporator is almost the same. As a result, the COP decreases with higher compressor power and the same cooling effect. Also, the COP increases as the blower setting increase for most of the cases. As the blower setting increases the load on the evaporator increases. Hence, the compressor has to work harder to achieve a higher cooling effect. If the increase in cooling effect is higher than the increase in compressor power, the COP increases, and vice versa.

4.2.4   Total power and fuel consumption

The total AC system power consumers are the compressor, the front and rear blowers and the electric fans. The electric fan is triggered by the condenser outlet pressure and the coolant temperature. According to the control mechanism, the electric fan is not triggered for all the steady-state simulations. So, the summation of the compressor power and the blower power is fed into the driveline model as engine loads to compute the overall fuel consumption. The electrical power consumptions of front and rear blower are provided by the supplier. The electrical power of the fan is supplied by the alternator which is driven by the engine.

By inputting the compressor power and the mechanical blower power into the driveline model, we can obtain the fuel consumption in the corresponding road profile. The simulation results for fuel consumption at constant road load and at 26.7°C and 32.2°C ambient temperatures are shown in Figure 4-5 and Figure 4-6. The fuel consumption rate (FCR) increases as the blower setting increases due to a higher load on the engine. However, the difference between AGS closed and open are minimal. In general, the FCR is always lower when the AGS is closed regardless of the blower settings. The figures also show the difference in the FCR by comparing AGS closed with AGS open condition. They reveal that the delta FCR decreases as the blower setting increases. This is because as the blower setting increases, the difference in compressor power increases too. Since the vehicle is operating at a constant speed, the aerodynamic benefit of having AGS closed is constant for all blower settings. As the blower setting increases, the overall benefit becomes smaller due to constant aerodynamic benefit and increasing compressor power consumption. The excess compressor power reduces the overall benefit in fuel consumption, but the reduction is not enough to justify opening the AGS. In general, closing the AGS at highway speed despite the blower setting offers better fuel economy. The highest reduction we can obtain in FCR is 0.06 L/100km when the AC load is the lowest. And the lowest reduction in FCR is 0.03 L/100km when the AC load is the highest. The results at constant road load, 32.2 °C ambient temperature show similar conclusions. It is interesting to see that with a higher increment in compressor power, the delta fuel consumption rate is higher at M3 blower mode by comparing to the results at Hi blower mode. This is because the fuel consumption map of the engine is not linear, therefore, the benefit in the fuel consumption rate is not inverse proportional to the increment in compressor power with AGS closed.

Steady-state driveline simulation results at 26.7°C
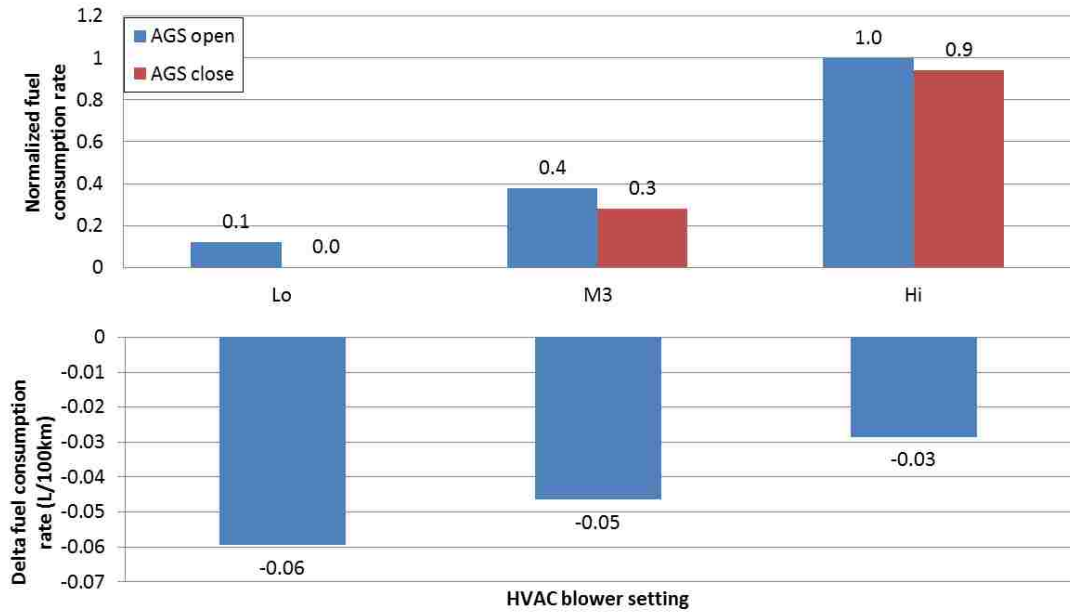
Figure 4-5: Steady-state simulation results from the driveline model at 26.7 °C. The graph above is the normalized fuel consumption rate, the graph below shows the delta fuel consumption rate by comparing AGS closed with AGS open condition.

Steady-state driveline simulation results at 32.2°C
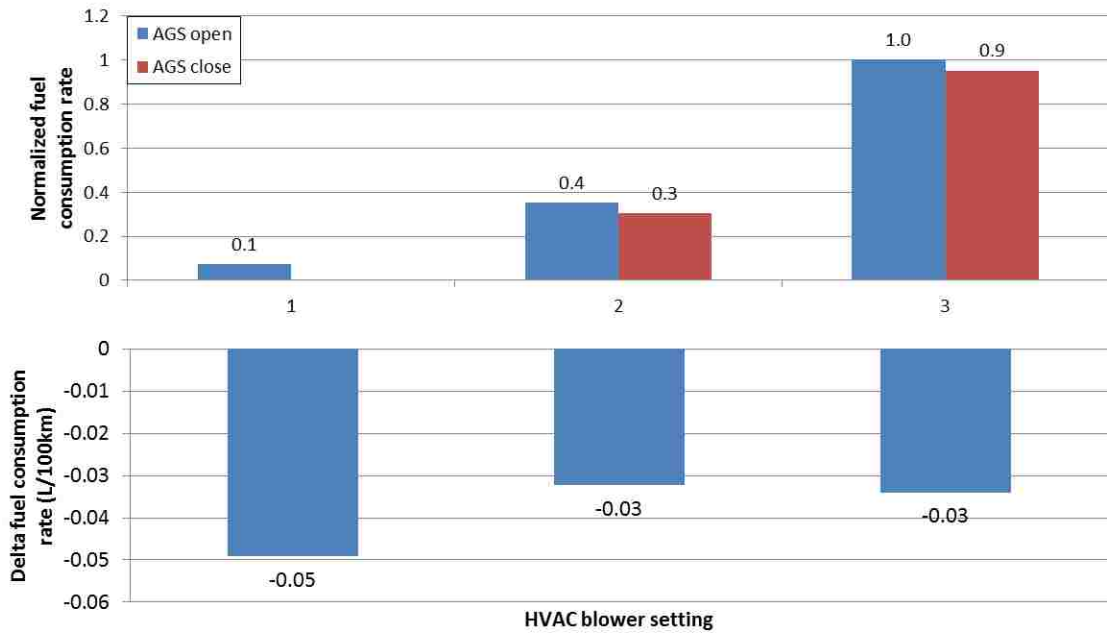
Figure 4-6: Steady-state simulation results from the driveline model at 32.2 °C. The graph above is the normalized fuel consumption rate, the graph below shows the delta fuel consumption rate by comparing AGS closed with AGS open condition.

4.3 Simulation of transient drive cycles

Due to simplicity, the blower setting is set at the high mode for all the drive cycle simulations. The reason for choosing Hi blower setting is that the AC load is the highest in this case, assuming the aerodynamic benefit is the same, the increment in compressor power is more likely to negate the aerodynamic benefit with AGS close. The objective here is to find out whether there is benefit in fuel economy without affecting the AC cooling performance when the AC has the largest cooling load. The results for the drive cycles are shown in Figure 4-7 and Figure 4-8. The average cabin temperatures for AGS open and AGS close are almost the same, which suggests that when AGS is in the closed position, the cooling performance is not affected by the insufficient air flow. Since the system is operated under fully recirculation mode, as the cabin air temperature decreases, the cooling load on the evaporator decreases along the cycle as well.

4.3.1 Compressor power consumption

The compressor power consumption for the cycle at 26.7°C is shown in Figure 4-7. In the beginning, since the vehicle speed is low, the compressor consumes more power to pump the refrigerant because of the insufficient air flow at the condenser surface. When the vehicle reaches highway speed, the condenser inlet air flow increases, the condenser refrigerant temperature decreases which also decreases the internal pressure. Hence the compressor power drops rapidly. In the highway speed segments, the compressor power remains almost constant; this is because the AC system is running under recirculation mode, the cabin air temperature decreases along the cycle and reaches almost constant at the end, which also suggests that the cooling load on the evaporator decreases and reaches almost constant. Therefore, the fluctuation of the compressor power consumption at the end is very small. The compressor power with AGS closed is almost double as the power at AGS open condition at the beginning of the cycle. The reason for this could be in the beginning, the condenser inlet air flow is too low with AGS closed, and the compressor has to consume extra power to increase the temperature of the refrigerant and enable the refrigerant to reject enough heat in the condenser. While with AGS open, even the condenser air flow is low, it is still enough for the condenser to work properly. When the vehicle reaches highway speed, the compressor power drops due to enough condenser air flow and the difference in the compressor power between AGS closed and AGS open becomes much smaller.

Simulation results for the drive cycle at 26.7°C
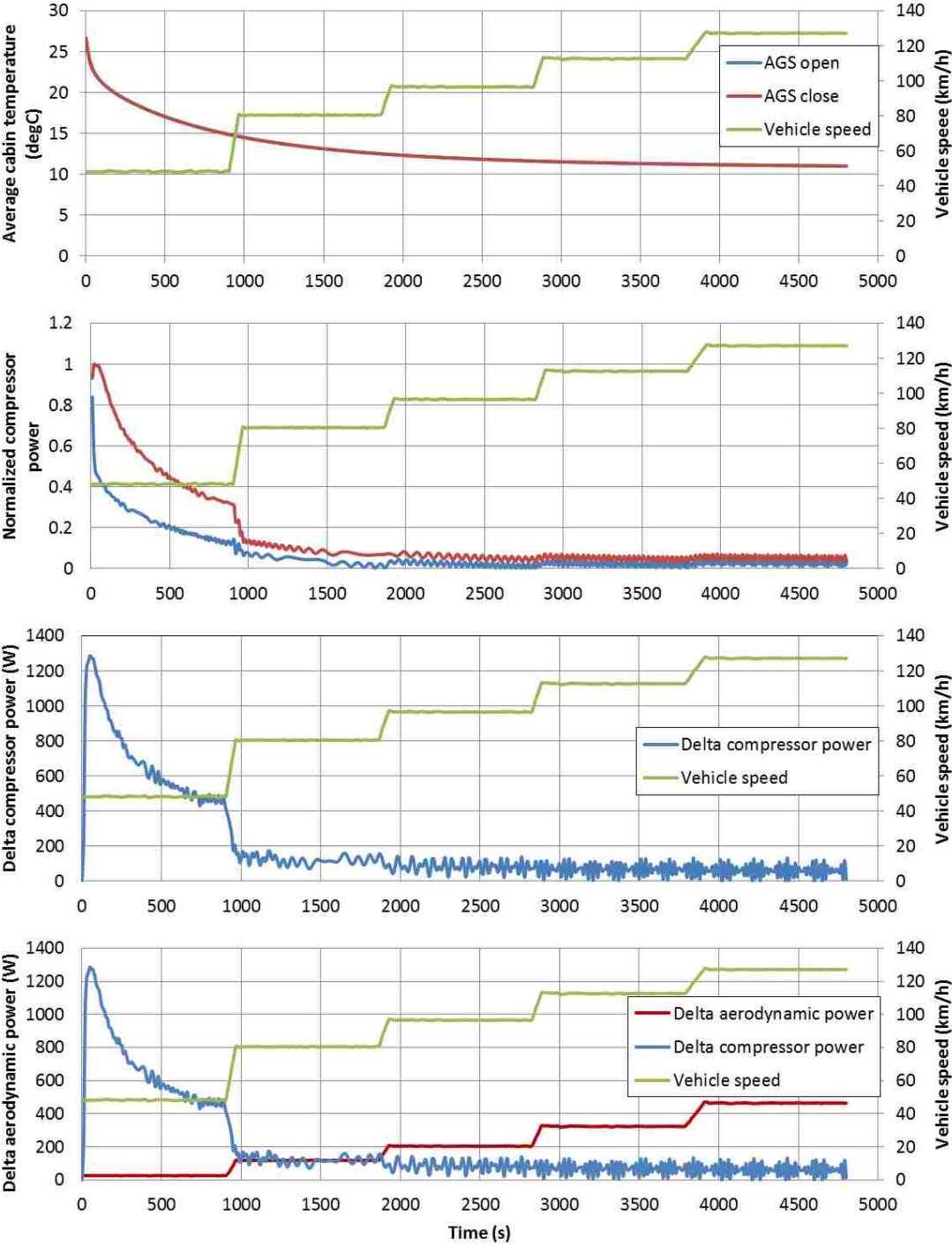
Figure 4-7: The transient drive cycle simulation results from the AC model at 26.7°C. The first graph shows the average cabin air temperature. The second figure shows the normalized compressor power. The third figure shows the delta compressor power by comparing AGS closed condition with AGS open condition. The last figure shows the tradeoff between the aerodynamic power and the compressor power. The aerodynamic power is calculated according to equation 2-1.

33

Simulation results for the drive cycle at 32.2°C

Figure 4-8: The transient drive cycle simulation results from the AC model at 32.2°C. The first graph shows the average cabin air temperature. The second figure shows the normalized compressor power. The third figure shows the delta compressor power by comparing AGS closed condition with AGS open condition. The last figure shows the tradeoff between the aerodynamic power and the compressor power. The aerodynamic power is calculated according to equation 2-1.
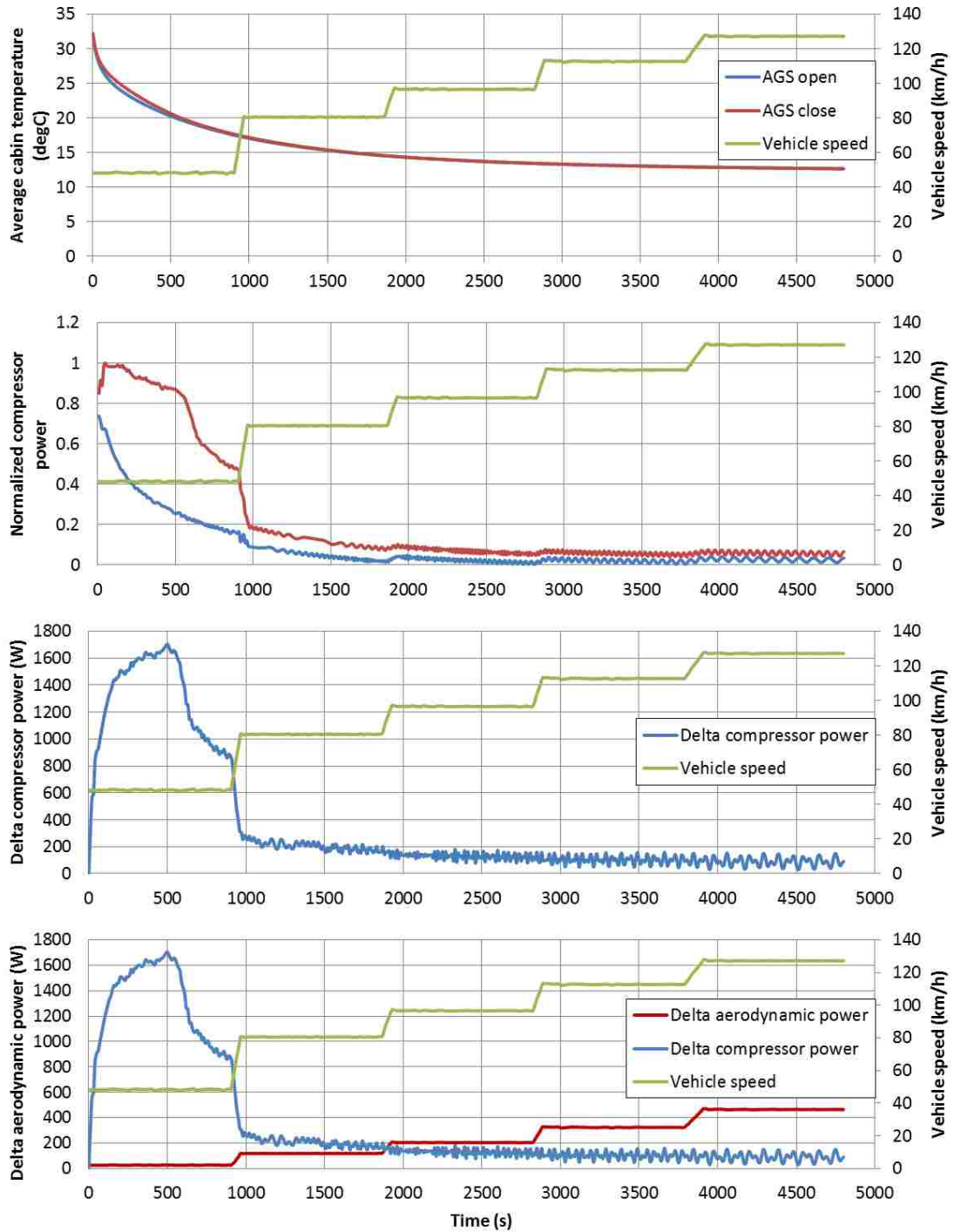
The results from Figure 4-7 show the compressor power difference value between the AGS closed and the AGS open condition. It shows that at the start the difference peaks at 1200 W and then drops to a constant at around 100 W. So, the compressor power is almost the same for AGS open and close condition at very high speed, the benefit due to aerodynamic performance with AGS closed could be outstanding during this region.

By comparing the results at 26.7°C and 32.2°C, the compressor power consumption is generally higher at a higher ambient temperature. With higher ambient temperature, the heat exchange rate between the ambient air and the condenser decreases and hence the compressor power will consume more power to lift the refrigerant pressure and temperature and increase the heat transfer rate to meet the constant cooling load on the evaporator side. At the low-speed range, the difference due to higher ambient temperature is significant especially for the AGS closed condition. In the highway speed segments, the impact of ambient temperature rise is relatively small.

4.3.2   Tradeoff between the AC compressor power and the aerodynamic power

Figure 4-7 and Figure 4-8 show the tradeoff between the AC compressor power and the aerodynamic power. The delta values are obtained by comparing AGS closed with AGS open condition. In the first speed segment at 26.7°C, the delta compressor power is much larger than the delta aerodynamic power. So, the AGS should remain open to avoid this peak in delta compressor power. In the second speed segment, the values are similar, so the AGS can be either open or closed. In the last three speed segments, the delta aerodynamic power is larger than the delta compressor power, therefore, the AGS should be closed.

The simulation results at 32.2°C show similar results. The AGS should be open in the first two speed segments, and it should be closed in the last three speed segments. The results for both 26.7°C and 32.2°C show that the critical vehicle speed is around 80 km/h where the AGS should be closed.

Since the delta aerodynamic power and the compressor power intersect in the transient section of the drive cycle at 32.2°C, further simulations are running with the vehicle speed ranging from 80 km/h to 93 km/h with three intermediate speeds and each segment lasts for 900 s. Similarly, for the cycle at 26.7°C, simulations are running with vehicle speed ranging from 68 km/h to 80 km/h. The results are shown in Figure 4-9. The result at 26.7°C shows that the threshold velocity is 77 km/h instead of 80 km/h. This suggests that the transient behavior of the system must be considered when designing the AGS control strategy. The result for 32.2°C shows that the critical

velocity is 84 km/h. However, the delta compressor power is still decreasing rapidly in this speed segment, so, the result might be different after the delta compressor power reaches almost a constant. Again, the transient behavior of the system has a large impact on the compressor power consumption and the critical vehicle speed. The critical speed obtained here is highly dependent on the cycle itself. The conclusions obtained from one drive cycle cannot be applied to another one.

From the results, it is worth noting at 32.2°C, the delta compressor power is relatively low in the beginning of the cycle. Since in the beginning, the load on the compressor is high with both AGS open and close conditions, if the compressor works under full load for both cases, then the delta power could be small. And then since the cooling load on the evaporator side decreases along the cycle due to decreasing cabin temperature, the compressor work consumption decreases consequently. With AGS open, the compressor power is decreasing faster than that with AGS closed, so the delta compressor power increases again.

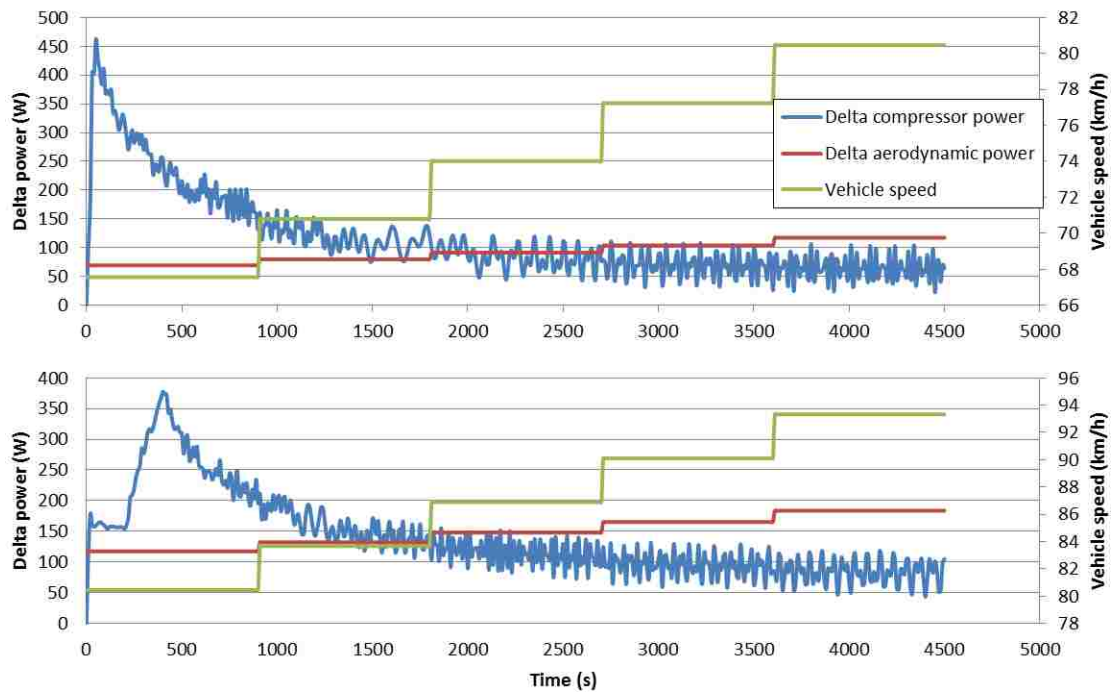*Figure 4-9: The tradeoff between the delta compressor power and the delta aerodynamic power at 26.7 ℃ and 32.2 ℃. The figure on top shows the result at 26.7 ℃.*

4.3.3   Impact of front-end air flow on the AC performance

The results include compression ratio, compressor displacement and COP are shown in Figure 4-10 and Figure 4-11. For both simulations, the compression ratio decreases along the cycle due

to the decreasing cooling load on the AC. But the compression ratio at 32.2°C is higher than that at 26.7°C.

Another parameter that also changes with the vehicle speed and has a significant effect on the compressor control system is the engine rpm. Since the compressor is belt-driven and coupled with the engine, the compressor speed is relative to the engine speed. Whenever there is a sudden vehicle speed change, the compressor speed changes too. So, the external controller adjusts the stroke according to the compressor rpm to reach a reasonable level of refrigerant flow rate. The compressor displacements are shown in Figure 4-10 and Figure 4-11. Generally, the compressor displacement decreases as the compressor speed increases. As the cooling load decreases and the compressor rotary speed increases along the cycle, the stroke must be reduced to decrease the refrigerant flow rate. One interesting section is when the vehicle speed increases from 48 km/h to 80 km/h. For the AGS open cases, the compressor displacement increases as the vehicle speed increases. The reason for this is that the compressor speed decreases due to gear shifting, to increase the refrigerant flow rate and meet the cooling demand, the compressor stroke length must increase. On the other hand, the compressor displacement continues decreasing in this section for AGS close cases. After that, the cooling load decreases for the rest of the cycle as the vehicle speed increases. As the compressor rpm increases, the compressor displacement must be decreased furthermore to meet the lower cooling demand. It is interesting to see that at the beginning of the cycle at 32.2°C, the compressor is working with full stroke length when the AGS is closed. This explains why the compressor power is so high during this section.

For all four simulation conditions, the COP follows the same trend. The COP increases and then decreases as the vehicle speed increases, and the peaks occur when the vehicle is at 80 km/h. At this speed, the AC system can consume the least energy to achieve the same cooling performance. In the first speed range where the vehicle speed is lower than 80 km/h, the condenser inlet air flow is low; this means that the compressor requires more power in this range. As the vehicle speed increases, the condenser inlet air flow increases and cools the condenser. The condenser temperature and pressure decrease accordingly. Consequently, the compressor power consumption decreases. The variable displacement compressor reduces the stroke length since it senses the reduction in the cooling load. The refrigerant flow rate decreases, and the cooling capacity of the evaporator decrease as a result. If the compressor power reduction is more significant than the cooling capacity reduction, the COP would increase, and vice versa. So, when the vehicle speed increases from 80 km/h, the reduction of the evaporator cooling capacity is more significant than the reduction in the compressor power consumption. Hence the COP drops.

Simulation results focusing on the AC performance for the drive cycle at 26.7°C
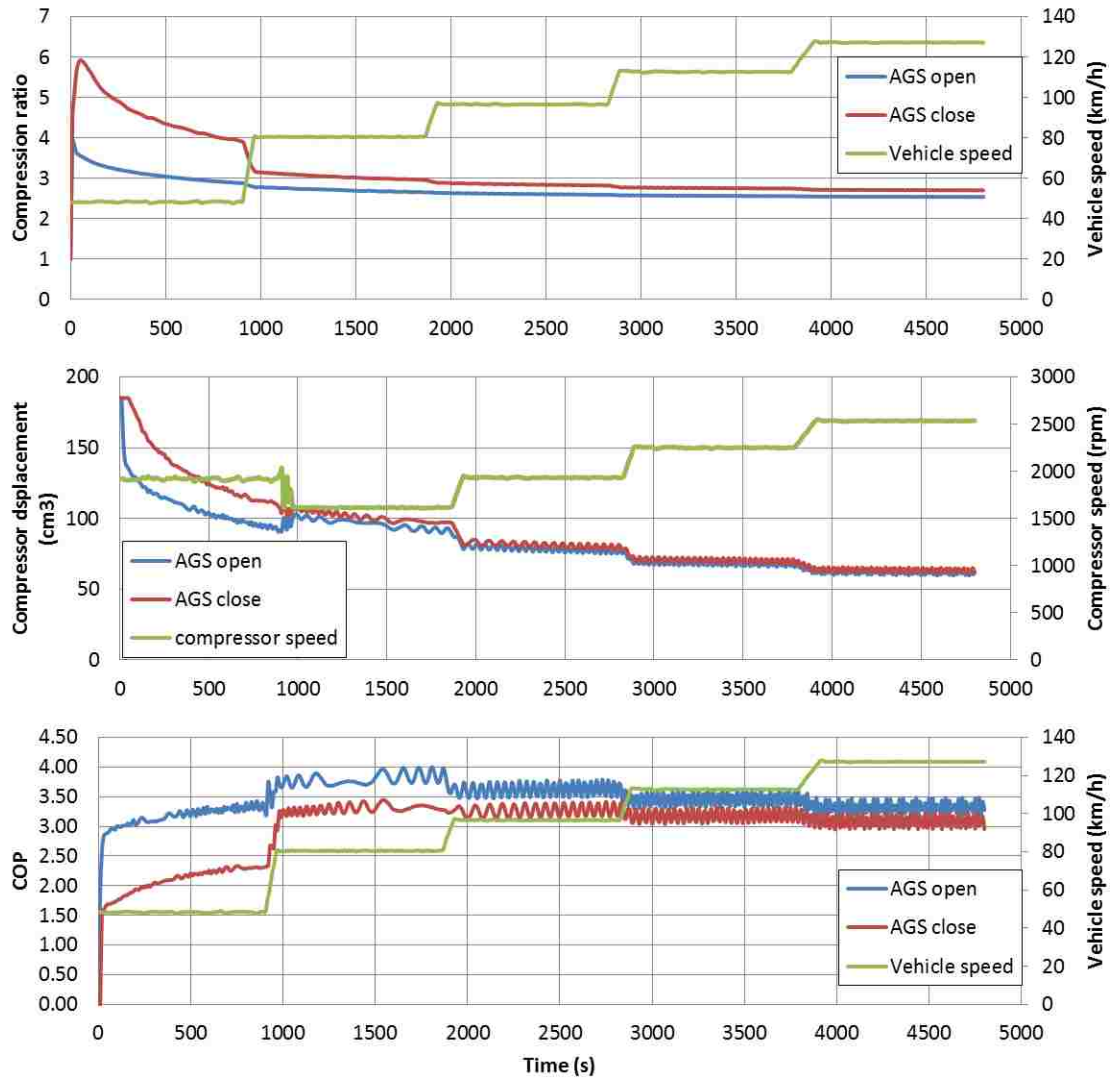
Figure 4-10: Simulation results focusing on the AC performance for the drive cycle at 26.7°C. The figure shows compression ratio, compressor displacement and the COP along the cycle at 26.7 °C.

Simulation results focusing on the AC performance for the drive cycle at 32.2°C
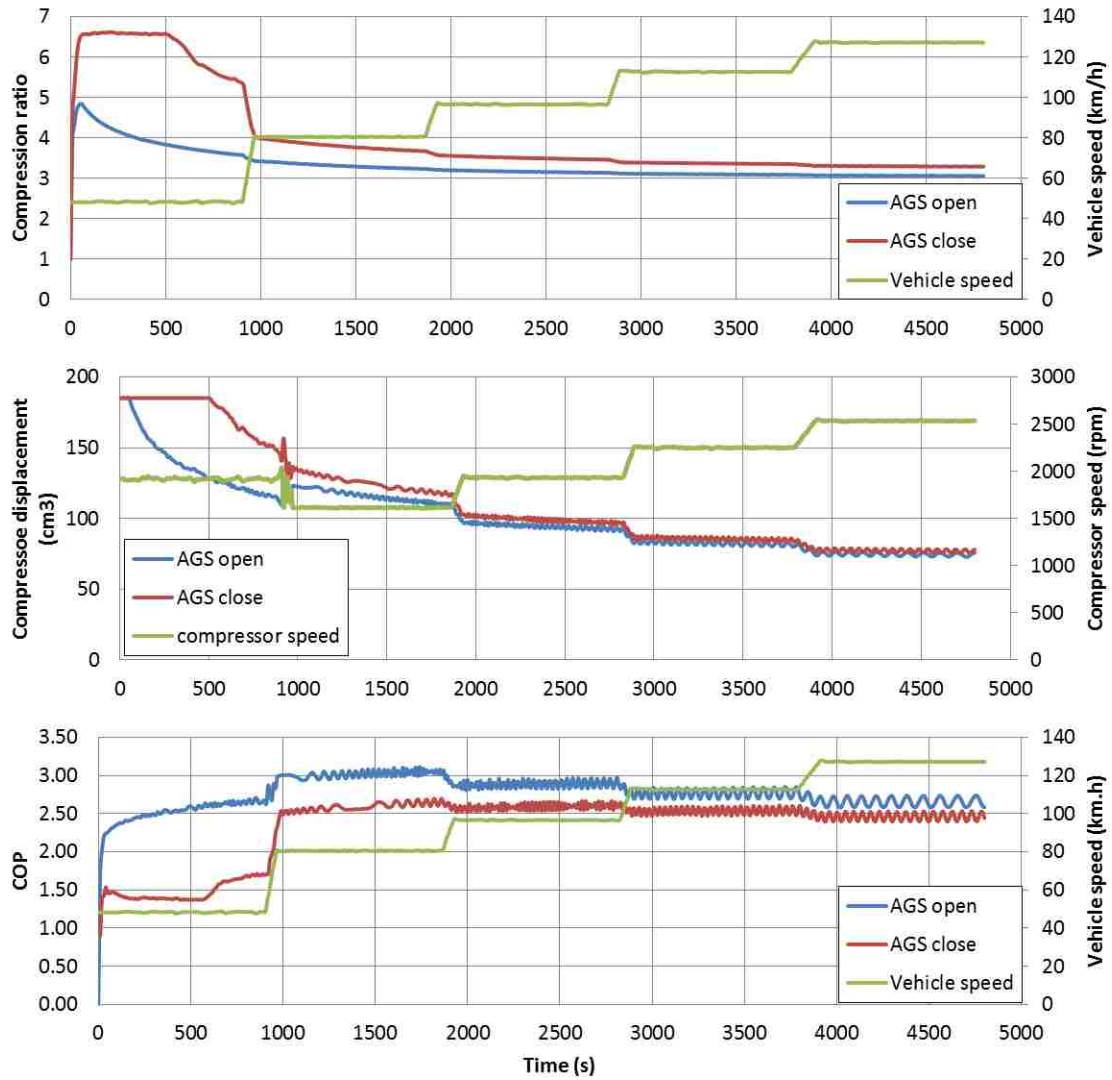
Figure 4-11: Simulation results focusing on the AC performance for the drive cycle at 32.2°C. The figure shows compression ratio, compressor displacement and the COP along the cycle at 32.2°C.

It is evident that the COP for AGS open is higher than AGS close. Due to insufficient front-end air flow, the condenser temperature and pressure increase when the AGS is closed. Eventually, the compressor power consumption goes up. As the increase in the evaporator cooling capacity is much smaller than the increase in the compressor power consumption, the COP drops.

It is also evident that the COP is higher with lower ambient temperature and with AGS open. Therefore, the AC system is more efficient under these two operating conditions.

4.3.4   Total power and fuel consumption

Figure 4-12 and Figure 4-13 show the simulation results of the fuel consumption for the cycle at 26.7°C and 32.2°C. Overall, the cumulated fuel consumption (CFC) is 0.02 L more with AGS open by comparing to the AGS closed case for the simulation at 26.7°C. However, Figure 4-12 shows that at the beginning the fuel consumption rate (FCR) is lower with AGS open instead of AGS closed, which suggests that the AGS should stay open and then switch to the closed position at a certain point to achieve lower fuel consumption.

To go into more details, the delta FCR and CFC by comparing AGS closed condition with AGS open condition are also plotted. In the first speed segment (48 km/h), the difference in FCR is positive, which means that the FCR with AGS open is lower than with AGS closed. In the second speed segment, the difference in the FCR fluctuates around zero. So, the AGS can be either open or closed since the difference is tiny. For the rest of the cycle, the difference becomes negative, and this suggests that the AGS should be closed to have smaller FCR and better fuel economy. It is worth noting that the delta FCR follows the similar decreasing trend as the compressor power difference as shown in Figure 4-7 and Figure 4-8. It suggests that the compressor power consumption plays an essential role in the AGS position optimization process. If the increment in the compressor power consumption is more significant than the aerodynamic drag improvement when the AGS closes, then the AGS should remain open.

For the cycle at 32.2°C, Figure 4-13 shows that the CFC is 0.04 L less with AGS open condition. Similar to the result for the cycle at 26.7°C, the result shows that at the beginning the FCR is lower when AGS is in open position instead of closed, and at the end, the FCR is higher when AGS is in open position. By comparing the cycle at different ambient temperatures, the one at 32.2°C generally consumes more fuel due to the higher ambient temperature. With AGS open, the CFC calculated at 32.2°C is 0.15 L more than the CFC at 26.7°C. And the increment in CFC as the ambient temperature increases while the AGS is closed is 0.21 L. In general, the impact on the fuel consumption due to temperature rise is more significant when the AGS is closed. As the results at 32.2°C indicate, with higher ambient temperature, the AGS should remain open in the first two speed ranges, and it should be closed for the rest of the cycle. Again, the delta FCR for the cycle at 32.2°C follows the similar decreasing trend as the delta compressor power as shown in Figure 4-8. The results for the drive cycle at both ambient temperature show that the critical vehicle speed is 80 km/h. In this drive cycle, if the vehicle speed is over 80 km/h, the AGS should certainly be closed. However, the result for 32.2°C shows that the critical speed may be higher than 80 km/h, which has been discussed in 4.3.3.

Driveline simulation results on the transient drive cycle at 26.7°C
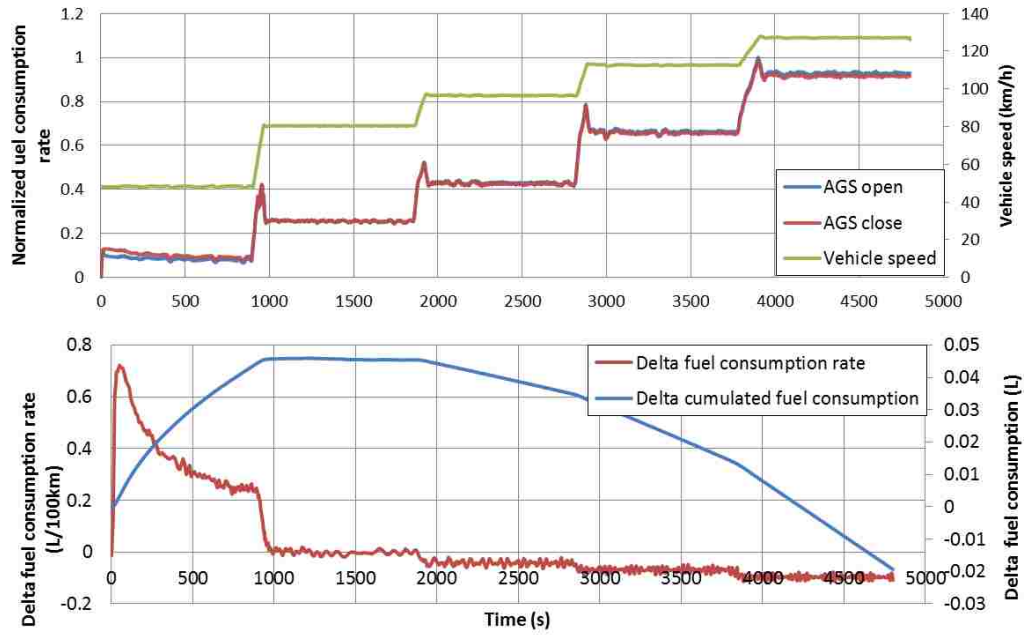
Figure 4-12: The driveline simulation results on the transient cycle at 26.7 ℃. The figure on the top shows the normalized fuel consumption rate, the figure on the bottom shows the delta fuel consumption rate by comparing AGS closed with AGS open condition.

Driveline simulation results on the transient drive cycle at 32.2°C
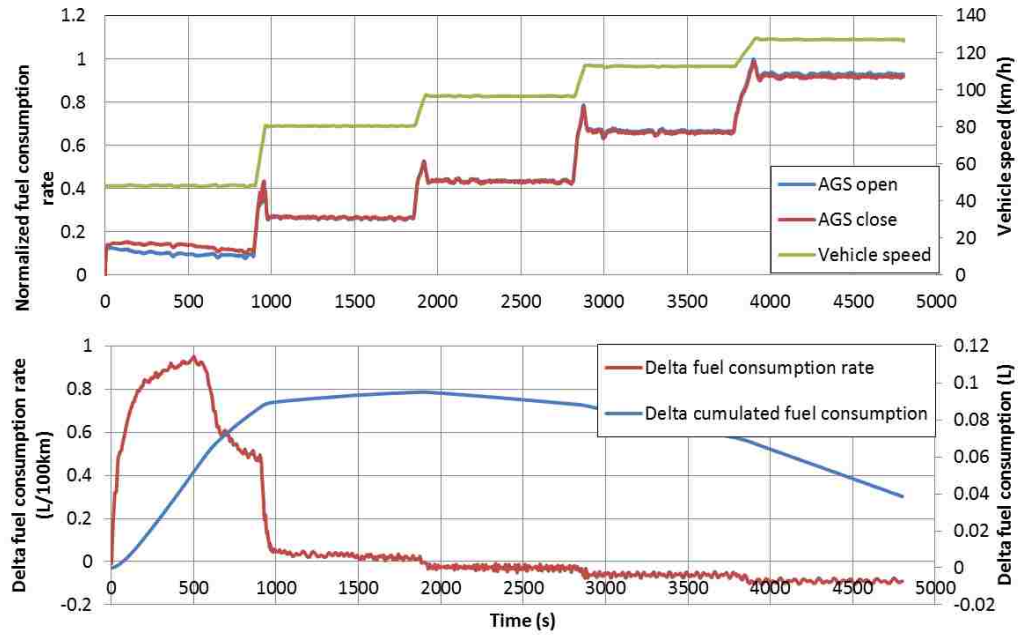
Figure 4-13: The driveline simulation results on the transient cycle at 32.2 ℃. The figure on the top shows the normalized fuel consumption rate, the figure on the bottom shows the delta fuel consumption rate by comparing AGS closed with AGS open condition.

41

4.3.5 AGS position determination

The delta FCR can be used to justify the AGS position. If delta FCR is positive, then the AGS should be open to have better fuel economy. For the cycle at 26.7°C and 32.2°C, the time to close the AGS is 1877 s and 1879 s, respectively. By comparing to the AGS open cases, the CFC improvements with the proposed AGS position are 0.7% and 0.6% for the cycle at 26.7°C and 32.2°C, respectively.

The potential benefit due to the AGS technology is further explained by computing the reduced fuel consumption by comparing the same vehicle driving from Windsor to Toronto with AGS fully open and fully closed at 26.7°C and 32.2°C. The saved fuel for the four-hour trip is 0.17 L and 0.13 L if the AGS remains closed for the whole trip under recirculation mode. Moreover, if we assume the vehicle is traveling at highway speed for the lifetime (300,000 km), the total saved fuel would be 128 L and 103 L. Overall, the benefit in fuel consumption by closing the AGS at highway speed is low when AC system is operating. Further considerations such as the performance of the cooling system must be taken into account when designing the control strategy, so the actual benefit in fuel economy by closing the AGS could be even lower. Another way to improve the fuel economy is to reduce the coefficient of drag furthermore by improving the seal when the AGS is closed. But it reduces the air flowing through the condenser which brings back the tradeoff dilemma. The critical time and critical vehicle speed obtained in this chapter are dependent on the cycle itself, they are affected by the transient behavior of the system. If another cycle is used for this study, the critical vehicle speed would be different.

CHAPTER 5 CONCLUSION AND FUTURE WORK

The method described in this thesis can be used to estimate the benefit in fuel economy because of AGS application in the design stage of the vehicle. Since much detailed information is needed to calibrate the AC and cabin model, this method can be used after the design of the geometry and interior of the vehicle is finished. The result helps the engineers to decide whether it is beneficial to include the AGS in the vehicle.

In terms of the tradeoff between the aerodynamic power and the compressor power, the benefit in aerodynamic power by closing the AGS is more significant at highway speed. However, the increment in compressor power by comparing AGS closed with AGS open decreases as the vehicle speed increases. The overall benefit in fuel consumption is larger at higher vehicle speed. The compressor power increases as the ambient temperature and the AC loads increase, and the impact of ambient temperature on delta compressor power is higher when the AC load is higher.

The driveline model simulation on constant road load shows that the increase in power consumption of the AC is not comparable with the power saved due to aerodynamic drag reduction. The optimum position of the AGS is closed at highway speed even with the highest AC load. The simulation on the drive cycles at 26.7°C and 32.2°C shows that with the highest AC load, the cooling performance is not affected by closing the AGS. The critical vehicle speed where the AGS should be closed for the cycle is 80 km/h. However, this value is cycle dependent. The improvement in the fuel consumption for both cycles by comparing to AGS open case is 0.7% and 0.6% respectively. So, the improvement is slightly higher with lower ambient temperature.

Also, since the critical speeds found for different cycles show different results, the transient behavior of the system must be considered when designing the AGS control strategy.

5.1 Future work

In the future, the AC and cabin model can be integrated with the driveline model for co-simulation. In this way, a controller can be introduced to determine the position of the AGS and generate a continuous AGS control mechanism to achieve the minimum fuel consumption. Another auxiliary load, the electric fan, can be introduced to complete the model. However, the electric fan is controlled by the temperature of the coolant and the condenser pressure; the engine cooling model must be included as well.

Overall, more work in an integrated system model that includes AC system, engine cooling system, driveline, AGS control and fan control will give more insight into the transient behavior and give an opportunity to optimize the control strategy.

REFERENCES

1. Reducing CO2 emissions from passenger cars - Climate Action - European Commission. (2017, February 16). Retrieved May 5, 2018, from https://ec.europa.eu/clima/policies/transport/vehicles/cars_en

2. Corporate Average Fuel Economy. (2018, March 27). Retrieved May 8, 2018, from https://www.nhtsa.gov/laws-regulations/corporate-average-fuel-economy

3. Lin, W., & Sunden, B. (2010). Vehicle Cooling Systems for Reducing Fuel Consumption and Carbon Dioxide: Literature Survey. SAE Technical Paper Series. doi:10.4271/2010-01-1509

4. Daly, S. (2006). Automotive air conditioning and climate control systems. Amsterdam: Elsevier.

5. Arora, R. C. (2012). Refrigeration and air conditioning. PHI Learning.

6. Çengel, Y. A., & Boles, M. A. (2016). *Thermodynamics: An engineering approach*. New York, NY: McGraw-Hill Education.

7. El-Sharkawy, A. E., Kamrad, J. C., Lounsberry, T. H., Baker, G. L., & Rahman, S. S. (2011). Evaluation of Impact of Active Grille Shutter on Vehicle Thermal Management. *SAE International Journal of Materials and Manufacturing,4*(1), 1244-1254.

8. Torregrosa-Jaime, B., Bjurling, F., Corberán, J. M., Sciullo, F. D., & Payá, J. (2015). Transient thermal model of a vehicles cabin validated under variable ambient conditions. *Applied Thermal Engineering,75*, 45-53.

9. Natarajan, S., S, S. K., Amaral, R., & Rahman, S. (2013). 1D Modeling of AC Refrigerant Loop and Vehicle Cabin to Simulate Soak and Cool Down. SAE Technical Paper Series.

10. 2018 Chrysler Pacifica - Family Minivan. (n.d.). Retrieved from https://www.chrysler.com/pacifica.html

11. Markowitz, M. (2011). Minimising total vehicle energy consumption by balancing the aerodynamic benefit of an active grille shutter and the power consumption of the air conditioning compressor. Vehicle Thermal Management Systems Conference and Exhibition (VTMS10), 513-521.

12. Pfeifer, C. (2014). Evolution of Active Grille Shutters. SAE Technical Paper Series.

13. Bouilly, J., Lafossas, F., Mohammadi, A., & Wissen, R. V. (2015). Evaluation of Fuel Economy Potential of an Active Grille Shutter by the Means of Model Based

Development Including Vehicle Heat Management. *SAE International Journal of Engines,8*(5).

14. Cho, Y., Chang, C., Shestopalov, A., & Tate, E. (2017). Optimization of Active Grille Shutters Operation for Improved Fuel Economy. SAE International Journal of Passenger Cars - Mechanical Systems,10(2).

15. **Imagine.Lab, LMS.** *Amesim Brochure*.

16. Tian, C., Liao, Y., & Li, X. (2006). A mathematical model of variable displacement swash plate compressor for automotive air conditioning system. International Journal of Refrigeration, 29(2), 270-280.

17. LMS Imagine.Lab. (2016). AMEHelp. Rev15.

18. Wang, T., Gu, B., Wu, B., Ma, H., & Qian, C. (2015). Modeling for multi-pass parallel flow condenser with the effect of refrigerant mal-distribution. International Journal of Refrigeration, 60, 234-246.

19. Eames, I. W., Milazzo, A., & Maidment, G. G. (2014). Modelling thermostatic expansion valves. International Journal of Refrigeration, 38, 189-197.

20. Cho, H., Lee, H., & Park, C. (2013). Performance characteristics of an automobile air conditioning system with internal heat exchanger using refrigerant R1234yf. Applied Thermal Engineering, 61(2), 563-569.

21. Gemin, Stephen. (2014) Transient and steady-state Mobile Air Conditioning operation with the Inclusion of and Internal Heat Exchanger. Electronic Theses and Dissertations. 5122.

    https://scholar.uwindsor.ca/etd/5122

22. ASHRAE. (2009), ASHRAE Handbook. Fundamentals, SI ed., ASHRAE, Atlanta, USA.

23. Swinbank, W. C. (1964). Long-wave radiation from clear skies. Quarterly Journal of the Royal Meteorological Society, 90(386), 488-493.

24. Scott, T.C., FCA Internal Report, 2011

25. LMS Imagine.Lab. (2016). Two Phase Flow Library Rev 15, Users Guide.

26. LMS Imagine.Lab. (2016). Air Conditioning Library Rev 15, Users Guide.

27. LMS Imagine.Lab. (2016). Thermal Library Rev 15, Users Guide.

28. LMS Imagine.Lab. (2016). Heat Exchanger Assembly Tool Library Rev 15, Users Guide.

APPENDIX A   AMESIM LIBRARY INTRODUCTION

AMESim has numerous libraries which contain a lot of sub-models in many physical domains. In this thesis, four main libraries are utilized; they are two-phase flow (TPF), air conditioning (AC), thermal and the heat exchange assembly tool libraries. A general description regarding each library and their capability are explained below based on the AMESim library manual [24-28].

As AMESim suggested, the two-phase flow, air conditioning, and thermal libraries are essential to construct the AC model; each library plays an important role in the model construction:

- The TPF library is composed of basic elements such as boundary conditions, sensors, ducts, pressure losses, and components to model refrigerant internal flow;
- The TH library which is used to model the heat exchanger wall thermal solid capacities and environmental moist air;
- The AC library that is composed of specific AC system global components.

The TPF library is composed of the following components:

- Thermodynamic and thermo-physical properties of refrigerant fluids and moist air
- Refrigerant and moist air sources for the application of boundary conditions
- Basic elements to model internal flow, internal heat exchanges with phase change
- Regular and singular pressure losses
- Basic elements to model the external heat exchanges between moist air and solid walls
- Look-up table efficiency compressors and expanders

For AC system simulation, it is undoubtedly that the properties of the two-phase flow have a strong impact on the simulation results. The AMESim two-phase flow libraries can provide a wide range of refrigerant properties and enable the user to model:

- Energy transport
- Internal convective heat exchanges
- External flow convective heat exchanges
- Pressure losses, temperature levels, mass flow rates and enthalpy flow rates distribution
- Gas mass fraction evolutions in the system
- Mass transfer between the vapor and the liquid phase

This library is used to provide refrigerant properties, sub-models of the ducts and piping, as well as some sensors which are used to check the thermal properties such as temperature, pressure or

enthalpy within the AC system. Different pre-defined correlations are available to calculate the heat transfer rate when modeling the heat exchangers [24], the details about the relative correlations for two-phase flow are included in APPENDIX B.

The AC library provides pre-defined sub-models of the main components within an AC system; this library is composed of:

- Compressors
- Thermal valves
- A receiver drier model
- Condenser components and evaporator components
- A Cabin Thermal Model
- Moist air source

These models can conduct transient and steady-state simulation to calculate the heat transfer between the ambient air and the solid walls. The AC model built in this thesis contains the variable displacement compressor, the TXVs, the receiver drier and the evaporator components from this library.

The thermal library provides thermal properties of solid materials and can calculate heat transfer between solid materials based on the basic heat transfer modes which are conduction, convection, and radiation. It contains 17 pre-defined solid material sub-models. If the material needed is not in the list, there is user-defined option to specify the properties of the required material. There are two types of components in this library, the resistive components and the capacitive components. The capacitive components are the masses or thermal capacities in which the temperatures are computed by putting the heat flow rate as the input. The resistive components are the components in which the heat flow rates are evaluated based on the traditional heat transfer modes from the temperature inputs; this implies that a thermal model is always built with resistive components connected by capacitive components. From this library, the thermal capacity sub-model is used to model the IHX by representing the aluminum tube that separates the hot and cold flow. The moist air sub-model provides the boundary conditions at the evaporator inlet in the AC system. By focusing on the heat transfer calculation, the air is regarded as 0-dimensional, and it represents the heat exchange between the evaporator fins and the moist air.

The main assumptions are listed below:

- The heat flow is one dimensional;

- The solids are considered isotropic, which means that their thermal properties are the same in all directions;
- The temperature in the thermal capacities is homogeneous.

The HEAT library is mainly aimed at the study of heat exchanger interactions within a closed environment, such as the HVAC system under the hood in case of automotive applications. Regarding application, this library can be used in any system where heat exchangers and related components interact through external fluid flow. This library is developed to help the engineers to get an initial idea of stack behavior at an early design stage, study the trade-off between different configurations and precisely evaluate the performance of the different fluid subsystems throughout an entire driving cycle. It also has a 3D visualization window to show the temperature and heat flux distribution of the heat exchanger frontal surface. In this thesis, the condenser is constructed by utilizing the HEAT library to precisely evaluate the condenser performance.

APPENDIX B   AMESIM AC MODEL SUB-MODELS

As explained in the previous section, AMESim is graphic based simulation software, which means it uses icons to represent sub-components that constitute the whole model. In this section, the main sub-models of the AC system are shown as icons and the main principles are explained.

Figure B- 1shows an icon that represents the properties of the R1234yf refrigerant that flows into the AC system. It has a built-in database which provides the thermal properties of the two-phase flow such as the density, the specific heat at constant pressure, the absolute and kinematic viscosities, the specific enthalpy, the thermal conductivity and so on. Thanks to this, the sub-model can calculate the total fluid mass and volume in the circuit, the critical temperature, pressure, and density. There are two ways to define the initial condition of this sub-model; the user can define the initial temperature and the weight of the refrigerant in the loop, if these parameters are not specified, the initialization of the state variables of the system is done in the sub-models composing the system.

Figure B- 1: AMESim icon for TPF_FP01 sub-model which defines thermodynamic properties for fluids, in this thesis, R1234yf is used as the refrigerant [24].

Another similar icon as shown in Figure B- 2 defines the thermal properties such as density, specific heat and conductivity for solid materials. There is a large predefined material library in AMESim; however, the user-defined material is also available if the desired material is not in the predefined list; this can be done in two ways. The user can either set the thermal properties as constant or identify the thermal properties as a function of temperature.

Figure B- 2: AMESim icon for sub-model THSD00 which provides thermal properties for solid materials, the user can use the pre-defined material, the user-defined material with constant thermal properties or the user-defined material with thermal properties vary with temperature [27].

B.1 Compressor sub-model

The sub-model ACVDCOMP03 is used to model the VDC with external regulation as Figure B- 3 indicated. This icon has four ports, the inputs for each port are:

- Port 1 - suction pressure and density at the inlet of the compressor
- Port 2 – control signal
- Port 3 - discharge pressure and density at the outlet of the compressor
- Port 4 - rotary speed of the compressor

The control signal is a number that ranges from 0 to 1. Where 0 means the compressor is at the minimum stroke; 1 means the compressor is at maximum stroke; and any other numbers indicate that the compressor stroke is in between.
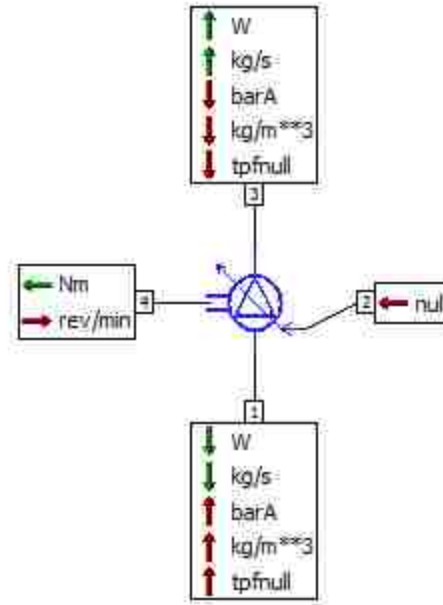
Figure B- 3: [ACVDCOMP03] Variable displacement compressor [26].

The outputs at port 1 and 3 are the mass flow rates and the enthalpy flow rates. The volumetric, isentropic and mechanical efficiencies must be specified to use this sub-model. Otherwise, the polynomial coefficient for mass flow rate and enthalpy loss has to be defined instead. So, the mass flow rate is obtained from the volumetric flow rate or directly from the volumetric flow rate if it is specified. In the presented model, the compressor sub-model is defined by specifying volumetric, isentropic and mechanical efficiencies as functions of the compressor rotary speed and the pressure ratio which is defined below:

$$x_p = \frac{P_{disc}}{P_{suct}}$$

Where

- P_{disc}: discharge pressure [PaA]
- P_{suct}: suction pressure [PaA]

The mass flow rate is calculated by using volumetric flow. The calculation is shown explained below.

At any instance, the compressor stroke can be calculated as:

$$disp = sig \cdot (disp_{max} - disp_{min}) + disp_{min}$$

Where

- disp: current compressor displacement

- sig: control signal at port 2

- disp$_{max}$: maximum compressor displacement

- disp$_{min:}$ minimum compressor displacement

The current volumetric efficiency is calculated as:

$$\eta_{vol} = (1 - sig) \cdot \eta_{vol\_min} + sig \cdot \eta_{vol\_max}$$

Where

- $\eta_{vol:}$ current volumetric efficiency

- η_{vol_min}: volumetric efficiency at minimum compressor displacement

- η_{vol_max}: volumetric efficiency at maximum compressor displacement

The mass flow rate at port 3 can be computed as follows:

$$\dot{m}_3 = \eta_{vol} \cdot \rho_s \cdot N \cdot disp$$

Where

- $\dot{m}_3$: mass flow rate at port3 [kg/s]

- ρ_s: refrigerant density at suction side [kg/m^3]

- N: rotary speed of the compressor [rpm]

By knowing the isentropic efficiency, the enthalpy flow rate can be calculated. The isentropic efficiency is expressed as follows:

$$\eta_{is} = \frac{h_{dis} - h_s}{h_d - h_s}$$

Where

- η_{is}: isentropic efficiency

- h$_{dis:}$ specific isentropic enthalpy at discharge [kJ/kg]

- h$_s$: suction specific enthalpy [kJ/kg]

- h$_d$: discharge specific enthalpy [kJ/kg]

The enthalpy increase across the compressor can be calculated as below:

$$\Delta h = h_d - h_s = \frac{h_{dis} - h_s}{\eta_{is}}$$

The enthalpy flow rate increase across the compressor can be calculated as:

$$\dot{m}h_{comp} = \dot{m}_3 \cdot \Delta h$$

Where $\dot{m}h_{comp}$ is the enthalpy flow rate increase [W].

The enthalpy flow rate at the suction (port1) is expressed below:

$$\dot{m}h_1 = -\dot{m}_3 \cdot h_1$$

Where h_1 is the specific enthalpy at suction, the value is obtained by knowing the suction pressure and suction density.

The discharge enthalpy flow rate at port 3 is equal to:

$$\dot{m}_3 h_3 = -\dot{m}h_1 + \dot{m}_3 \cdot \Delta h$$

Finally, the mechanical efficiency is used to compute the torque at port 4 and the equation is expressed as below:

$$\eta_{mech} = \frac{\dot{m}_3 \cdot \Delta h}{T_4 \cdot N}$$

Where

- η_{mech}: mechanical efficiency
- T_4: compressor torque at port 4 [Nm]

The volumetric and isentropic efficiencies are specified as 2D maps, while mechanical efficiency is assumed as constant with a value of 0.8.
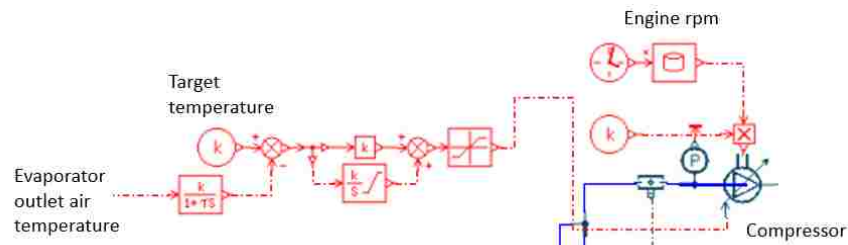

Figure B- 4: Variable displacement compressor model with an external regulator in AMESim.

The VDC and the external regulator model are shown above. The external regulator model is a controller that compares the evaporator outlet temperature with a predefined target temperature. The controller adjusts the stroke length to minimize the difference between these two temperatures.

B.1 Condenser sub-model

In this section, the construction and calibration of a tube and fin condenser model are described. The condenser model has to consider the external gas side the refrigerant side and the solid walls and the fins, have the ability to model non-homogeneous air velocity or temperature distribution on the frontal area of the condenser, and also accurately model the evolution of refrigerant pressure, temperature, gas mass fraction along the condenser. For the simplicity of the AC loop modeling, the condenser for simulation has an integrated receiver/dryer. Both geometric data and experimental data are needed to ensure that the condenser model functions properly. In AMESim, it has a unique way to describe the condenser geometry. As illustrated in Figure B- 5, the structural configuration of a tube and fin condenser is shown in the upper image and the detailed geometry of the fins which are defined in AMESim is shown below. The geometric data is used to calculate the thermal capacity of the tube walls and fins, the heat exchanger surface areas, the cross-sectional area and hydraulic diameters. Hence the mass flow rate of the external and internal flow can be determined by knowing the parameters above and consequently the heat exchange within the condenser can be computed.
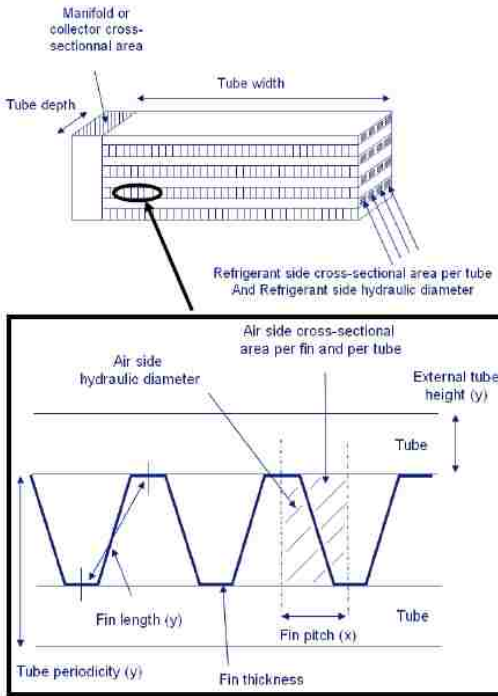
Figure B- 5: AMESim condenser geometry definition for a parallel flow condenser. The upper image shows the configuration of a parallel flow tube and fin condenser with the parameters labeled. The refrigerant flows along the tube width while the air flows between the fins. The lower image shows the detailed configuration of the fin structure, and important parameters are labeled [28].

A three-path tube and fin condenser model in AMESim is shown in Figure B- 6. Three main parts constructed the model: the external air flow, the internal refrigerant flow and the condenser walls and fins. All the components are described in the following paragraph.
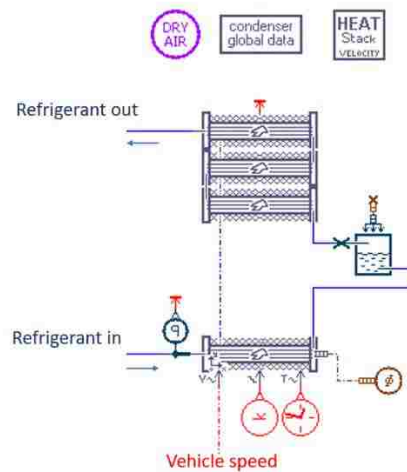

Figure B- 6: The four-pass condenser with an integrated receiver model in AMESim.

Start with the external flow that passes through the condenser, since moisture is not considered in the HEAT library, so the gas property is defined in the pneumatic library as a single gas or a mixture of dry gases. In this case, dry air is used, and the corresponding icon is shown below. The gas properties are defined completely using the perfect gas constant and three polynomial functions giving the absolute viscosity, the specific heat at constant pressure and the thermal conductivity [16].

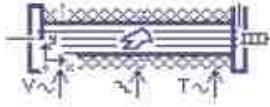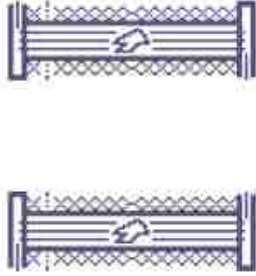*Figure B- 7: AMESim sub-modle PN_AIR defines dry air properties [16].*

One crucial aspect of the condenser model is that the port is only available for internal flow; the external flow connection is invisible. A plug-in sub-model which is used to define the external flow property, and the sub-model is called HEAT Gas Stack and the icon is shown in Figure B- 8. The sub-model serves as an intermediate element which associates the external flow with the HEAT components, in this case, is the input to the condenser model.

Figure B- 8: AMESim sub-model HEAT01, serves as a plug-in tool which manages the external flow interactions between the HEAT components. An index has to be assigned to this index of the stack, and the same external flow properties will be applied to other components that have the same index of the stack. If more than one stack is used, an additional plug-in element has to be put on the sketch with a different index of stack assigned [28].

The walls and fins of the condenser are constructed by several sub-models and they are listed in Table B- 1. This tube and fin condenser is composed of four passes: one reference pass, two intermediate passes, and one top pass. Each pass is a set of tubes in which the direction of the refrigerant is the same. The elementary geometric information such as the sizes of the collector, tube, and fin are defined in the condenser geometric data sub-model HEATPFHE002, while the other information such as condenser position, the number of passes and the air velocity and temperature profile is defined in the reference pass of the condenser.

Table B- 1: Sub-models and descriptions of the condenser [28].

Sub-model name and type		Note
	HEATCONDREF120 The reference part of a condenser	The reference part is mandatory since it contains the geometric information such as the position, number of passes and it communicates the information with the plug-in element
	HEATCONDINT110 HEATCONDINT120 The intermediate part of a condenser	Two intermediate passes are available because of the different internal flow ports location
	HEATCONDTOP120 The top part of a condenser	The top pass defines the first pass of the condenser

As mentioned in the table above, the reference pass of the condenser model contains geometric information such as the condenser position, the tube numbers in each pass, the material of the walls and fins, the external flow, and the air velocity and temperature profile on the condenser frontal surface. There are several ways to define the velocity and temperature profile. The velocity can be defined as homogeneous constant, or a 2D map file which defines the velocity distribution on the frontal area, or homogeneous variable where the velocity is described by an input signal, or a 3D map file which defines the velocity distribution on the condenser frontal surface changes along with car speed. The similar setting also applies to temperature data. When calibrating the integrated AC and cabin model against the CCD test or other transient simulations, the velocity and the temperature data in condenser are defined with 3D map files which determine the velocity and temperature distribution on the condenser frontal area with the vehicle speed as the control signal. For simulation under steady state, the air velocity and temperature are set as homogeneous constant and ambient constant correspondingly, where the velocity and temperature

are uniform across the frontal area as constants. Important user-defined parameters are listed in Table B- 2.

Table B- 2: User-defined overall geometric parameters and external air profile in the reference pass in the condenser model.

Parameter	value	Note
Width	0.704m	None
Height	0.510m	None
Thickness	0.016m	None
Tube number for pass 1	28	None
Tube number for pass 2	19	None
Tube number for pass 3	14	None
Tube number for pass 4	9	None
Velocity data	Map file + control signal	3D map file for air velocity profile with vehicle speed as the control signal
Temperature data	Map file + control signal	3D map file for air temperature with time as the control signal

Another sub-model is the condenser global data HEATPFHE002, and the AMESim icon is shown in Figure B- 9. All the other geometric data that is not defined in the above table is defined in this sub-model, such as the fin geometry, the collector cross-sectional area, the hydraulic diameter of the internal and external flow and so on. It serves as a global data center which defines the geometric data for all the passes sub-models in one attempt. This sub-model is also responsible for computing the mass of the solid material and the heat exchange.

Figure B- 9: AMESim sub-model HEATPFHE002 defines the elementary condenser geometric data, heat transfer correlations [28].

The heat transfer of the condenser model is calculated by considering the following heat transfer: the internal convective heat transfer, the conductive heat transfer in the condenser walls, the

external heat transfer between the wall and the air. All the heat exchanges are calculated based on specific correlations. All the geometric information and the correlations which are defined in the condenser global data are listed as follow:

Table B- 3: Heat transfer and pressure drop correlations for the condenser.

Title	Correlation	Note
Condensation correlation	Shah correlation	Calculates the internal convective heat exchange in the case of condensation
Boiling correlation	VDI for horizontal tubes correlation	Computes the internal convective heat exchange in the case of boiling
External heat transfer correlation	Nusselt correlation	Computes the external convective heat transfer
Two-phase flow frictional pressure drop correlation	Mac Adams correlation	Calculates the frictional pressure drop for the two-phase flow

All the internal flow parameters such as the hydraulic diameter of the internal flow are provided by the suppliers. All the internal surfaces of the tubes are assumed to be smooth, so the absolute roughness is zero. These parameters are used to characterize the internal flow and internal heat exchange.

The dimensions of the tubes and fins are also provided, and these values are used to compute the mass of solid material, hence the solid wall thermal capacity.

The external parameters that are relevant to external convective heat exchange such as the external hydraulic diameter, enables the model to compute the convective exchange surface and the total air-cross-sectional area.

By considering the internal refrigerant flow, the mass flow rate in the refrigerant resistive element is calculated by the reference part of a condenser HEATCONDREF120 using Bernoulli's formulation as below:

$$\dot{m} = \rho c_q A \sqrt{\frac{2\Delta P}{\rho}}$$

Where

$\dot{m}$: refrigerant mass flow rate [kg/s]

ρ: density of the refrigerant computed at upstream condition [kg/m3]

c_q: flow coefficient

A: refrigerant flow path area [m^2]

ΔP: pressure difference across the resistive element

The flow coefficient is calculated based on the friction coefficient in the pipe and the flow condition such as laminar or turbulent flow. The external air volumetric flow rate is calculated by multiplying the imposed air velocity with the frontal area of the condenser.

The internal convective heat transfer between the wall and the refrigerant is calculated as follows:

$$\dot{Q}_{int} = h_{int} \cdot A_{int} \cdot (T_{ref} - T_{wall})$$

Where h_{int} is the internal convective heat transfer coefficient in W/(m2·K), A_{int} is the heat transfer area between the refrigerant and the wall in m^2, T_{ref} is the refrigerant temperature, and T_{wall} is the wall temperature at that instant. The value of the internal convective heat transfer coefficient highly depends on the condition of the refrigerant. It can be divided into four conditions: single-phase laminar flow, single-phase turbulence flow, two-phase condensation, two-phase boiling. For single-phase laminar flow condition, the computation is as follows:

$$h_{int,lam} = Nu_{int,lam} \times \frac{\lambda}{Dh}$$

Where λ is the refrigerant thermal conductivity in W/(K·m), Dh is the hydraulic diameter on the external air side.

$$Nu_{int,lam} = 3.66$$

The Nusselt number remains constant in laminar regime, and the value depends on the geometry of the heat exchanger. 3.66 is the typical value of circular duct geometry.

For single-phase turbulent flow, the Gnielinski correlation is used to compute the convective heat exchange. The equations are shown below:

$$h_{turb} = \frac{\left(\frac{\xi}{8.0}\right) \cdot (Re - 1000)Pr}{1 + 12.7\sqrt{\frac{\xi}{8.0}} \cdot [Pr^{2/3} - 1.0]} \times \frac{\lambda}{Dh}$$

Where ξ is the friction coefficient, Re is the Reynolds number, Pr is the Prandtl number; λ is the refrigerant thermal conductivity in W/(K·m), Dh is the hydraulic diameter on the external air side. The friction coefficient can be calculated from the Churchill expression for single phase flow:

$$\xi = 8\left[\left(\frac{8}{Re}\right)^{12} + \left(\left[2.457ln\left(\frac{1}{[7/Re]^{0.9} + 0.27(\frac{\varepsilon}{D})}\right)\right]^{16} + [37530/Re]^{16}\right)^{3/2}\right]^{1/12}$$

Where ε is the mean surface roughness, and D is the internal flow hydraulic diameter.

For two-phase flow, the model considers two flow conditions: condensing and boiling. In the AC model, the Shah correlation is used to calculate the heat transfer during condensation and VDI for horizontal tubes correlation is used to calculate the heat transfer during boiling. More details can be found in [24].

The external heat exchange between the air and the solid wall is calculated as follow:

$$\dot{Q}_{ext} = h_{ext} \cdot A_{ext} \cdot (T_{air} - T_{wall})$$

Where h_{ext} is the external convective heat transfer coefficient in W/(m2·K), A_{ext} is the heat transfer surface area between the air and the wall in m^2, T_{air} is the air temperature and T_{wall} is the solid wall temperature at that instant. The h_{ext} value also depends on the air flow condition since it is proportional to the Nusselt number, it is computed as below:

$$h_{ext} = Nu_{ext} \times \frac{\lambda_{ext}}{Dh_{ext}}$$

Where Nu_{ext} is the Nusselt number of the external flow, which is air in this case, λ_{ext} is the thermal conductivity of air, Dh_{ext} is the hydraulic diameter on the external side. The Nusselt number can be computed in two ways depends on the air flow condition (laminar or turbulence). When the flow is in the laminar regime, the Nusselt number is constant; when the flow is turbulence, the Nusselt number is calculated from the Prandtl number and the Reynolds number and then multiplied by the finned surface effectiveness.

McAdams correlation is used in this model to calculate the friction coefficient and hence the pressure drop across the condenser. This correlation treats the homogeneous two-phase flow as a

single-phase processing mean fluid proper. Other fundamental assumptions for the homogeneous flow are: there is no slip between the two phases and thermodynamic equilibrium between the phases. By knowing the average viscosity of the homogeneous flow, AMESim calculates the friction coefficient and hence the pressure drop across the refrigerant pipe. The McAdams correlation is shown as:

$$\frac{1}{\mu_{TPF}} = \frac{x}{\mu_v} + \frac{1-x}{\mu_l}$$

Where x is the gas mass fraction, it is defined as the ratio of the mass of vapor to the total mass of the mixture. μ_{TPF} is the mean viscosity of the homogenous flow, μ_v is the viscosity of the vapor and μ_l is the viscosity of the liquid.

The condenser model has a built-in receiver drier; the corresponding AMESim sub-model is shown in Figure B- 10. This sub-model serves as temporary storage for excess refrigerant when the cooling load is low. The height of liquid inside the receiver is monitored, and the liquid/vapor interface is referenced concerning the height of the hydraulic port located on port 3 in the AMESim icon. The outputs of the sub-model are chamber temperature, liquid volume percentage, and the refrigerant charge.
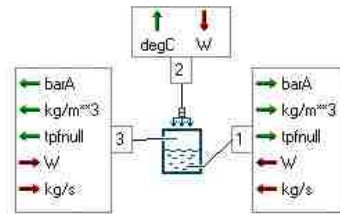

Figure B- 10: AMESim sub-model TPFSCH00 is a stratified chamber with an imposed heat flow rate which is useful for modeling accumulator or receiver [24].

B.2 Thermal expansion valve

The thermal expansion valve is a device that ensures fluid expansion and regulates the superheat at the evaporator outlet. The detailed description regarding externally equalized TXV working mechanism can be found in 3.2.3. The AMESim sub-model ACTEVSB02 is used to model the TXV, and the corresponding icon can be found in Figure B- 11. The port 1,2,3,4 labeled in the figure is connected to the evaporator inlet, evaporator exit, compressor inlet and condenser exit

correspondingly. Port 1 is the TXV outlet port, where it controls the amount of refrigerant flows into the evaporator. As described in 3.2.3, the valve lift depends on the force balance acting on the diaphragm. So, the valve can be closed entirely where the mass flow rate at port 1 equals to zero; the valve can be partially open where the current valve lift is used to calculate the mass flow rate, or the valve can be totally open, and the maximum valve lift is used to calculate the mass flow rate. Port 2 is used to get the information of pressure at the evaporator outlet. Port 3 provides refrigerant mass flow rate and enthalpy flow rate for the compressor inlet refrigerant flow and port 4 receives refrigerant pressure and density as input.
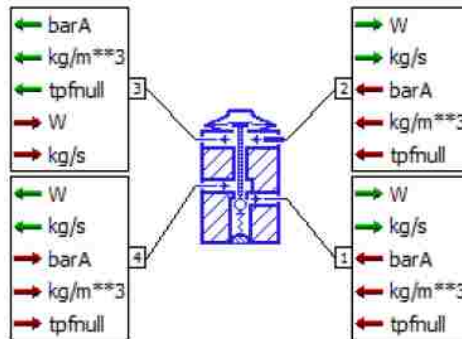
Figure B- 11: AMESim sub-model ACTEVSB02 can be used to model the thermostatic expansion valve with an integrated thermal sensing bulb [26].

The characteristic of the TXV is normally described in a four-dimension diagram provided by the supplier:

- The refrigerant saturation curve and calve opening curve as a function of thermal sensing bulb fluid in quadrant 1;
- The evaporator outlet pressure as a function of the valve lift for different constant temperature values in quadrant 2;
- The evolution of the reference mass flow rate as a function of the valve lift in quadrant 3;
- The evolution of the reference mass flow rate as a function of the evaporator outlet pressure in quadrant 4.

These curves are related to each other. For example, by knowing the 1st and 3rd quadrant, the 4th quadrant curve can be deduced. To calibrate this sub-model, the first three quadrants are required as inputs to have the correct set of parameters. A pressure offset at 0 °C models the

preload of the spring, by adjusting this value; it shifts the charging characteristic up and down in the first quadrant so that the model will mimic the actual TXV behavior. Other parameters such as reference pressures and reference subcooling temperature are required to be specified by the user. The important parameters of the front TXV sub-model in the AC model are listed in Table B- 4. The rear TXV is modeled and calibrated in the same method. The first three curves must be inputted as 2D map files in the model.

Table B- 4: Important parameters of the thermal expansion valve sub-model.

Title	Value	Note
Bulb temperature	43.33 degC	The initial bulb temperature equals the ambient temperature
Maximum valve lift	0.65 mm	Provided by the supplier
Reference high pressure	9.7 barA	Provided by the supplier
Reference low pressure	3.7 barA	Provided by the supplier
Reference subcooling	3 degC	Provided by the supplier
Pressure offset at 0 degC	1 barA	Models the spring preload
Time constant	10s	Represents the thermal inertia of the bulb

The output of the sub-model is the refrigerant mass flow rate at the outlet which is port 1. The calculation is as follows:

$$\dot{m}_1 = \dot{m}_{ref} \cdot \frac{\rho}{\rho_{ref}} \cdot \sqrt{\frac{P_4 - P_1}{P_{h,ref} - P_{l,ref}} \cdot \frac{\rho}{\rho_{ref}}}$$

Where $\dot{m}_{ref}$ is the mass flow rate at reference condition in kg/s, ρ is the upstream fluid density in kg/m³, ρref is the reference density computed from the reference pressure and reference subcooling. P4 and P1 are the pressure at port 4 and port 1 respectively. $P_{h,ref}$ and $P_{l,ref}$ are the reference high and low pressure at TXV inlet and outlet respectively.

B.3 Internal heat exchanger

The internal heat exchanger is a double-pipe device that enables the heat exchange between the refrigerant at the evaporator outlet and the condenser outlet and utilizes the energy that would

otherwise be wasted. The hot liquid refrigerant at the condenser outlet is cooled by the cold vapor at the evaporator outlet in the IHX, and while the liquid refrigerant flows through the evaporator, it can absorb more heat. The solid wall between the hot and cold flow serves as a heat exchanger, this part can be simply modeled by a thermal mass. The simplified IHX configuration is shown in Figure B- 12.
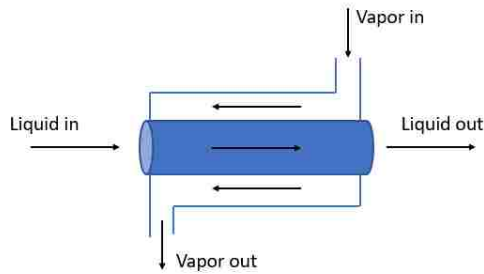

Figure B- 12: An illustration of a concentric tube type of heat exchanger which resembles the internal heat exchanger.

The AMESim model for the IHX is shown in Figure B- 13. It is composed of a thermal mass that represents the solid wall that separates the hot and cold flow and two pipes that are able to calculate the pressure drop along the IHX and amount of heat exchange. This configuration also resembles the concentric tube type heat exchanger shown above.

Figure B- 13: AMESim internal heat exchanger model.

One component of this model is the sub-model THC000, the AMESim icon is shown in Figure B- 14. It is a thermal capacity; the type of material and mass are user-defined parameters. It computes the temperature changing in the solid wall. The temperature dynamics resulting from the energy balance are calculated as follow:

$$\frac{dT}{dt} = \frac{\sum_{i=1}^{4} \dot{q}_i}{m \cdot c_p}$$

65

Where $\dot{q}_i$ is the input heat flux at the corresponding port in W, m is the mass of the solid material in kg, c_p is the specific heat of the material at temperature T in J/(kg·K).
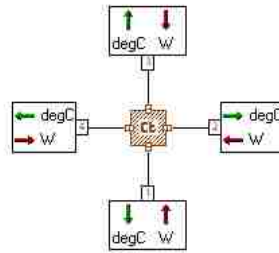

Figure B- 14: AMESim sub-model THC000 models a thermal capacity with the mass and material defined by the user [27].

The other component is the sub-model TPFPHE0001which models a two-phase flow pipe with friction and convective heat exchange. The sub-model computes the pressure drop and heat transfer along the pipe, and it handles both single-phase flow and two-phase flow. When calculating the pressure drop for single-phase flow, Churchill correlation is used to compute the friction coefficient. For two-phase flow, a list of the correlations is available to model the friction coefficient. Another option is that the pressure drop can be defined by an external user-defined function. In the simulation in the present work, Mac Adams correlation is used to model the friction coefficient for two-phase flow, the equations of the above correlations can be found in 0. As for heat exchange calculation, Gnielinski correlation is used to compute the convective heat transfer for single-phase condition. For the two-phase flow condition, two different situations are considered. Within the sub-model, a test is done to check if condensation or boiling occurs. When boiling occurs, VDI for horizontal tube correlation is used. When condensation occurs, Shah correlation is used to calculate the heat transfer coefficient. For more information regarding the correlations, please see reference [24].
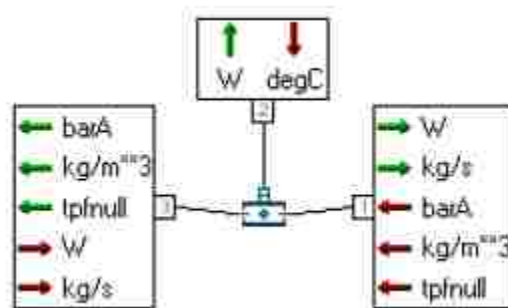

Figure B- 15: AMESim sub-model TPFPHE0001 is a two-phase flow pipe with friction and heat exchanger [24].

The convective heat transfer between the fluid and the wall is calculated as follows:

$$\dot{Q}_{conv} = hA_c(T_1 - T_2)$$

Where

$$A_c = \frac{4 \cdot A_{cross} \cdot le}{D_h}$$

- $\dot{Q}_{conv}$: convective heat flow rate [W]
- h: convective heat exchange coefficient calculated at the fluid temperature at the fluid temperature at port 1 [W/m²·K]
- T1: the temperature at port 2 which represents the wall temperature
- T2: the temperature at port 1 which represents the fluid temperature inside the pipe
- Ac: the convective exchange surface area of the pipe [m²]
- Across: cross-sectional area of the pipe [m2]
- Le: pipe length [m]
- Dh: hydraulic diameter of the pipe [m]

The geometric parameters of this IHX model are listed in Table B- 5. The mass of material does not affect the performance of the internal heat exchanger during steady-state simulation; it only affects the transient behavior.

Table B- 5: Geometric parameters of the internal heat exchanger AMESim model.

Title	Value	Note
Mass of material	0.25 kg	The mass of the thermal capacity
Temperature	43.33 degC	The initial temperature is the ambient temperature
Length	1 m	Length of the pipes
Cross-sectional area	176 mm²	The cross-sectional area of the pipes
Hydraulic diameter	15 mm	The hydraulic diameter of the pipes

B.4 Evaporator

There are two evaporators in this AC model. The front one has the plate and fin structure while the rear one has the tube and fin structure. The main difference between these two configurations is that the shape of the refrigerant channel is different, one is square, and one is round. Nevertheless, both evaporator models must model the refrigerant, the heat exchanger walls and the external air flow, which is very similar to the condenser model as described in 0. Moreover, they must model the non-homogeneous air velocity profile on the evaporator surface as well as the evolution of the refrigerant pressure, temperature and gas mass fraction along the evaporator.

1. Front evaporator sub-model

The front evaporator is constructed in AMESim as a U-shape plate and fin heat exchanger model. It is different from the condenser model in a way that the evaporator model considers the moist in the air. If the AC system is running at fully recirculation mode, the air that recirculates back into the evaporator will carry a high portion of moist, and this is not negligible. In the full recirculation mode of the AMESim model, the moist air property is provided by the cabin thermal model. And the air property at the evaporator outlet is provided as input into the cabin model to form the recirculation loop. When building the evaporator model in AMESim, both geometric and performance data are required. The geometric parameters are essential when computing the refrigerant mass flow rate, internal and external heat exchange, while the performance data is used to calibrate the model so that it will mimic the real-world evaporator performance. AMESim has its own way to define the plate-fin evaporator geometric parameters; they are illustrated in Figure B- 16 and Figure B- 17.
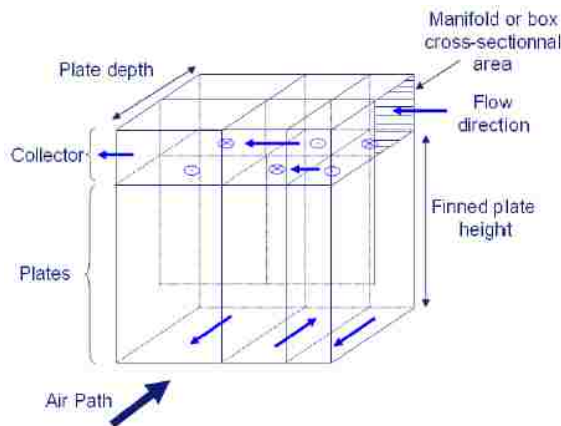

Figure B- 16: The overall configuration of the plate-fin evaporator with important elementary geometric parameters labeled in AMESim [16].
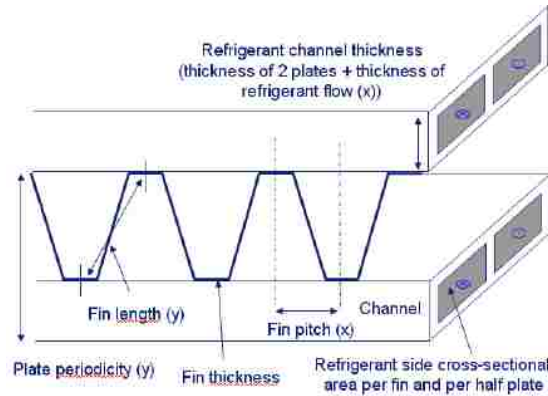
68

Figure B- 17: The detailed plate and fin configuration with important geometric parameters labeled in AMESim [16].
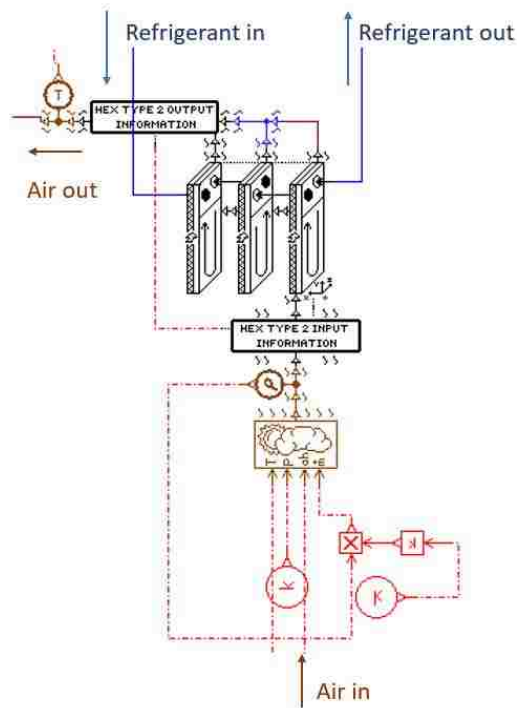

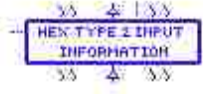*Figure B- 18: The front evaporator model in AMESim with refrigerant and air flow direction indicated. The refrigerant flows along the blue line.*

The main components of the front evaporator model are listed in Table B- 6. Since the plate-fin evaporator is divided into three passes, they are modeled by the reference pass, intermediate pass and end pass in the AMESim model. The other two sub-models ACINFOHEXT2IN0000 and ACINFOHEXT2OUT000 are used to define the inlet air profile and computing the outlet air properties respectively. Then the moist air source is used to impose a moist air flow as an air side boundary condition for the evaporator.

Table B- 6: Front evaporator sub-models in AMESim and descriptions.

Sub-model name and type		Note
	ACHEXT2REF2SO32 Super-component of a reference pass for heat exchanger	It is the reference pass for the plate-fin evaporator, and it is mandatory to use
	ACHEXT2INT2S032 Super-component of an intermediate pass for heat exchanger	It is the intermediate pass for the plate-fin heat exchanger. Depends on the number of passes in the evaporator, more than one intermediate pass can be used
	ACHEXT2END2S032 Super-component of an end pass for heat exchanger	It is the end pass for the plate-fin evaporator. It gives the moist air outlet condition of the pass
	ACINFOHEXT2IN0000	It is compulsory to use this sub-model to model the non-homogeneous mass flow rate profiles on the heat exchanger surface
	ACINFOHEXT2OUT000	This sub-model calculates the global information in the heat exchanger such as total heat flow rate or sensible heat flow rate
	THMAS00 Moist air source	It is used to impose a moist air flow on the evaporator inlet

It is different from the condenser components as described before; the elementary geometry needs to be specified in each of the super-component. Also, by comparing to other sub-models in the

70

AC library, each super-component has an additional moist air port which is used to monitor the outlet moist air properties coming from each pass. As mentioned before, the model has to model the evolution of the refrigerant condition and the pressure drop along the evaporator; this is done by dividing the pass into three volumes, and these volumes are connected with resistive frictional losses components. Literature correlations are used to calculate the pressure loss and internal heat exchange across each volume either in single and two-phase conditions. The super-components ACINFOHEXT2IN0000 and ACINFOHEXT2OUT000 are compulsory to use when building the plate-fin evaporator model since the first one calculates the first interpolation of the air flow profile to model the non-homogenous air flow rate profile on the evaporator surface, the second super-model computes the heat flow rate or sensible heat flow rate. Moreover, it calculates the moist air information at the outlet; hence the cabin model is connected at the output port during recirculation mode. The moist air source sub-model simply provided the moist air properties at the evaporator inlet. In this sub-model, air is assumed as 0-dimension flow where there is no pressure drop across this sub-model. The humidity ratio at the sub-model input can be either relative humidity or absolute humidity, and these values can be imposed when simulating under fresh mode or provided by the cabin thermal model when simulating under recirculation mode. However, the air mass flow rate must be an imposed value. When calibrating the integrated AC and cabin model against the CCD test, the blower setting is set at the highest mode. Constant air mass flow rates are imposed at the front and rear moist air source sub-models.

Literature correlations are used to calculate the pressure loss across the evaporator, the internal and external heat transfer. Please find the correlations used in the evaporator models in Table B- 7. Like the condenser model, different correlations are used when calculating the internal heat exchange. There are three cases in general: single-phase flow in the laminar regime, single-phase flow in laminar regime and two-phase flow. Under the two-phase flow condition, Shah Correlation is used in the case of condensation and VDI for vertical tubes correlation is used in the case of boiling. Due to the orientation of the evaporators, VDI for vertical tubes correlation is used instead of the horizontal tube one. The external convective heat transfer is computed more complexly by comparing to the condenser model since the distribution of the moist air flow rate is non-homogeneous on the evaporator surface.

Title	Correlation	Note
Condensation correlation	Shah correlation	Calculates the internal convective heat exchange in the case of condensation.
Boiling correlation	VDI for vertical tubes correlation	Computes the internal convective heat exchange in the case of boiling for the vertical flow path.
External heat transfer correlation	Nusselt correlation	Computes the external convective heat transfer.
Two-phase flow frictional pressure drop correlation	Mac Adams correlation	Calculates the frictional pressure drop for the two-phase flow.

The important geometric parameters on the refrigerant side are used to calculate the internal heat transfer surface while computing the internal convective heat transfer between the refrigerant and the solid wall. The fin and plate geometric parameters are provided by the supplier. This information is used to calculate the fin efficiency, the external exchange surface and hence the external heat exchange between the air and the solid wall.

The mass flow rates and the enthalpy flow rates in all the intermediate resistive elements are calculated in the pass super-components. The mass flow rate is calculated using Bernoulli's formulation as below:

$$\dot{m} = \rho c_q A \sqrt{\frac{2\Delta P}{\rho}}$$

Where ρ is the refrigerant density computed at upstream conditions, c_q is the flow coefficient, A is the refrigerant flow path area, ΔP is the pressure difference in the resistive element. The flow coefficient is calculated from the friction coefficient in a pipe, and the coefficient is a function of the relative roughness of the pipe and the flow condition.

A test is done on the upstream gas mass fraction of the fluid to calculate the enthalpy flow rate. Depends on the gas mass fraction, the density and the viscosity will be calculated in either single-phase flow conditions or two-phase flow conditions. If the gas mass fraction is equal to 0 or 1, the

density and viscosity are calculated for the liquid or the gas. If the gas mass fraction is between 0 and 1, the calculation is done for two-phase flow. And hence the enthalpy flow rate is calculated by multiplying the mass flow rate by the specific enthalpy of the flow calculated at the upstream condition. As for the computations for the internal and external heat exchange, the process is very similar to the condenser model. The same correlations are chosen as the condenser model except for the boiling process. Please refer Table B- 7 to see the correlations used under different conditions.

2. Rear evaporator sub-model

The rear evaporator is a tube-fin heat exchanger; it is constructed with the same process as the front evaporator. The only difference is that they have different internal configurations, the AMESim geometric definition regarding tube and fin heat exchanger is illustrated in Figure B- 19.
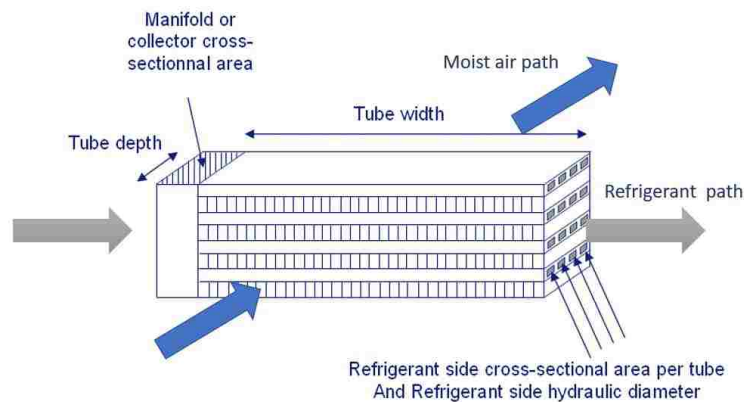
Figure B- 20: AMESim geometric definition regarding tube and fin heat exchanger [16].

The model is constructed in AMESim as the Figure B- 20 shown. The refrigerant flows along the blue line and the moist air flows along the brown line as indicated in the figure. It is able to model the external moist air side, the internal refrigerant side and the solid wall of the heat exchanger. The rear evaporator model has four passes: one reference pass, two intermediate passes, and one end pass. One moist air source and two information sub-models are also included. The information sub-models are used to interpolate the non-homogenous air distribution on the evaporator surface and to calculate the air condition at the outlet. The information of the sub-models is listed in Table B- 8.

Table B- 8: Rear evaporator sub-models in AMESim and descriptions

| Sub-model name and type		Note
	ACHEXT1REFS032 Reference pass for heat exchanger	None
	ACHEXT1TOP2S032 End pass for heat exchanger	None
	ACINFOHEXT1IN0000	It is compulsory to use this sub-model to model the non-homogeneous mass flow rate profiles on the heat exchanger surface
	ACINFOHEXT1OUT000	This sub-model calculates the global information in the heat exchanger such as total heat flow rate or sensible heat flow rate
	THMAS00 Moist air source	It is used to impose a moist air flow on the evaporator inlet
	TPFMADMG000 Conversion tool	Converts a mass flow rate into mass flow rate per unit surface
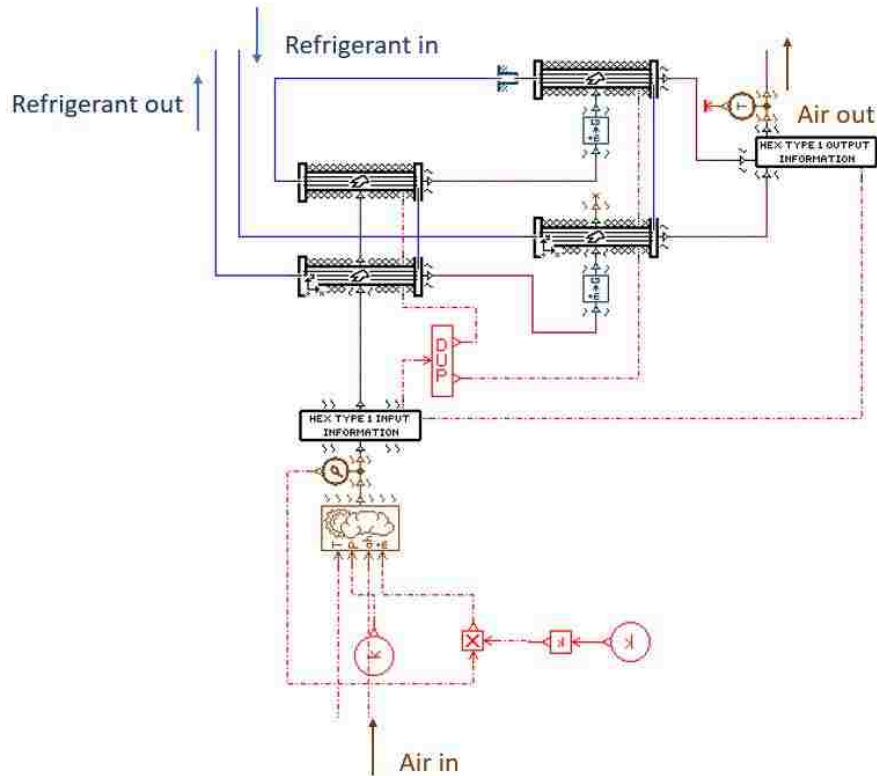
Figure B- 21: Rear evaporator model in AMESim.

The reason for using the conversion sub-model to convert the mass flow rate into mass flow rate per unit surface is that in AMESim, the variables and the units of the variables in each sub-model are pre-defined. For example, ACHEXT1REFS032 is the reference pass in the rear evaporator model, and it is shown in Figure B- 21. There are seven ports in total, the red arrows represent inputs, and the green arrows are outputs. All the variables have predefined meaning and units. At port 3, the unit for the flow rate is in kg/s. While at port 1, the input should have the unit in $kg/s/m^2$. The conversion sub-model is used to convert kg/s into $kg/s/m^2$.

Figure B- 22: AMESim sub-model ACHEXT1REFS032 is a reference pass of the tube-fin heat exchanger with all the units of variables labeled, red arrows are inputs while green ones are outputs [26].

The calculations for heat exchanges are the same as the front evaporator. However, when calculating the heat transfer within the solid wall, the geometric information is considered so that for tube-fin configuration is different from the plate-fin configuration. The correlations used for heat transfer and pressure loss calculations are the same as the correlations used for the front evaporator. The geometric parameters are provided by the supplier. The calculations for internal and external heat transfer is the same as the front evaporator, please refer to the first section in this chapter.

APPENDIX C   AMESIM CABIN MODEL

When modeling the AC system under the recirculation mode, the evaporator inlet air temperature and humidity depends on the net energy transfer inside the cabin. It is essential to evaluate the heat transfer in the cabin correctly to obtain the evaporator inlet air properties and thus ensure the accuracy of this model. The model is calibrated against the CCD test, so the heat transfer modes need to be considered are heat conduction, heat convection, and solar radiation through different opaque and other surfaces. For building the model, a lumped-parameter method is used, detailed geometric information of the vehicle cabin is needed as well as the thermal properties of all the material. As mentioned in the AMESim library introduction, most of the properties are provided in AMESim, the rest are provided by the supplier. The model can be run along to simulate the warm-up process, or it can be connected with the AC system to simulate the cool-down process.

One important feature of this cabin model is that it is divided into two thermal volumes since there are two evaporators in the AC system. However, when considering the heat transfer, the

cabin is treated as one whole volume to interact with other surfaces. The cabin air is connected to other surfaces by considering heat convection. For other multi-layer surfaces such as floor and carpet, door (composed by the outer surface, air gap, and the interior) and tailgate (also composed by the outer surface, air gap, and interior), heat conduction is considered in these surfaces. The solar load transferred through opaque or semi-transmitted surfaces is also considered.

For more details, the cabin model in AMESim is presented in Figure C- 1; a lumped-parameter method is used to build this model. The cabin components are simplified into thermal masses, and each possesses its own thermal properties, additional geometric data such as area and thickness are needed for the model to calculate the heat transfer. The thermal masses included in this model are the roof, dashboard, doors, floor and carpet, instrument panel, windshield, sunroof, and windows. All the thermal masses are interacting with the cabin air independently. The details of the heat exchange process will be described later in this section. First, the important AMESim icons in Figure C- 1 are explained as follows.
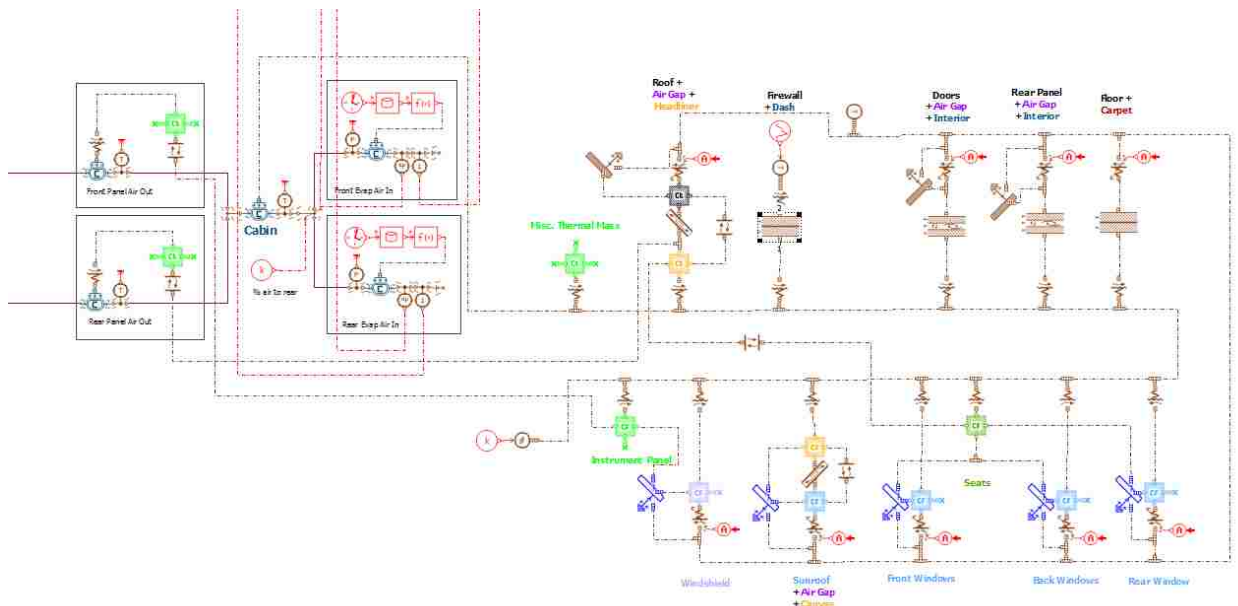
Figure C- 1: AMESim cabin model constructed with the lumped-parameter method. The lumped-parameters are thermal masses, and they are labeled in the figure above. In the first row from left to right, the included thermal masses are the roof, firewall and dashboard, doors, tailgate, floor, and carpet. In the second row from left to right, there are instrument panel, windshield, sunroof, windows, and seats.

The cabin itself is represented by a moist air chamber in AMESim, and the corresponding icon is shown below. It is used to calculate the temperature and the absolute humidity in a volume. The initial temperature, humidity, pressure and the chamber volume must be specified to use this sub-model.
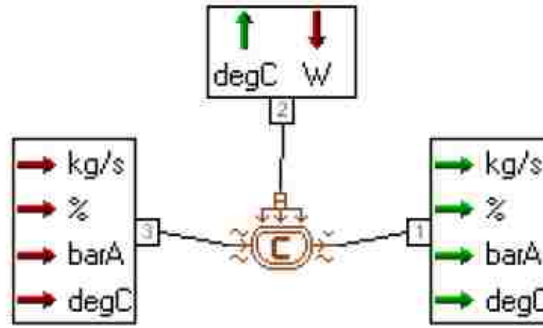
Figure C- 2: AMESim sub-model THMAC00, this moist air chamber sub-model is useful to model high volume such as a vehicle cabin or a house, which considers the dynamic behavior of the temperature and the absolute humidity in a constant volume space [27].

At port 1, the mass flow rate and humidity are outputs; at port 2, the heat flow rate is input, and the model calculates the temperature as output. At port 3 the mass flow rate, relative humidity, the pressure and the temperature are inputs. The dynamic changing of temperature and the absolute humidity are calculated as follows:

$$\frac{dah_{out}}{dt} = \frac{(1 + ah_{out})\left(\dot{m}_{ma} \cdot \left(\frac{ah_{in} - ah_{out}}{1 + ah_{in}}\right) + \dot{m}_w\right)}{\rho_{out} \cdot vol}$$

Where

- $\frac{dah_{out}}{dt}$: derivate of the absolute humidity at the outlet [$kg_{water}/kg_{dryair}/s$]
- ah_{in}: absolute humidity at the inlet [kg_{water}/kg_{dryair}]
- ah_{out}: absolute humidity at the outlet [kg_{water}/kg_{dryair}]
- $\dot{m}_{ma}$: moist air flow rate [kg/s]
- $\dot{m}_w$: water production rate [kg/s]
- ρ_{out}: density at outlet condition [kg/m^3]
- vol: volume of the chamber [m^3]

$$\frac{dT_{out}}{dt} = \frac{\dot{m}_{ma} \cdot \left(h_{ma,in} - h_{ma,out}\right) + \dot{m}_w\left(Lv + h_{v,out} - h_{ma,out}\right) + \varphi)}{\rho_{out} \cdot vol \cdot cp_{out}}$$
$$- \frac{(Lv + h_{v,out} - h_{da,out})}{cp_{out} \cdot (1 + ah_{out})^2} \frac{dah_{out}}{dt}$$

Where

- $h_{ma,in}$: inlet moist air specific enthalpy [J/kg]

- $h_{ma,out}$: outlet moist air specific enthalpy [J/kg]

- $h_{da,out}$: outlet dry air specific enthalpy [J/kg]

- $h_{v,out}$: outlet water vapor specific enthalpy [J/kg]

- Lv: water vapor latent vaporization heat [J/kg]

- φ : heat flux in [W]

- Cp_{out}: outlet moist air specific heat at constant pressure [J/kg/K]

Some thermal masses are modeled by the sub-model THC000. It is a sub-model of fixed thermal capacitance which can compute the temperature changes with respect to incoming heat flux. The corresponding AMESim icon is shown in Figure B- 14. Other thermal masses are by sub-model THDYNWALL, which is a dynamic sub-model representing a thermal wall with multiple layers. The layers can be made of different materials which also include air. The sub-model accounts for the heat conduction between solid layers, heat convection between the air and the solid wall as well as the radiation between the solid walls separated with an air layer. The AMESim icon is shown in Figure C- 3.
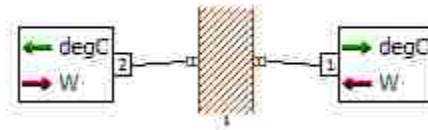
Figure C- 3: AMESim sub-model THDYNWALL models a wall made of multiple layers [27].

Between the cabin air and each thermal mass, there is the convective heat transfer. This is accomplished by connecting the cabin air and each thermal mass with a sub-model THGCV2. In this sub-model, different settings can be chosen according to the wall geometry and heat transfer correlations. Moreover, both natural and forced convective heat transfer are considered. The corresponding AMESim icon is shown below.
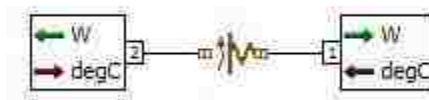
Figure C- 4: AMESim sub-model THGCV2 models the convective heat transfer between a fluid and a material [27].

To model the experimental condition of the CCD test, the solar load is not negligible. This part is modeled by sub-models THRSOL002 and THRSOL001. The AMESim icon is shown in Figure C- 5 and Figure C- 6. The first one is a general sub-model of solar radiation on the opaque surface

such as the roof, and the other one is to model solar radiation on the transparent surface such as the windshield. Both of the sub-models consider the solar incidence angle and the radiative effect due to the Stephan-Boltzmann law.
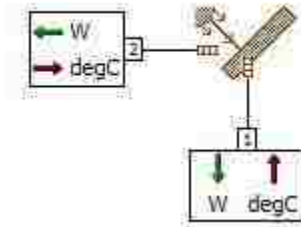

Figure C- 5: AMESim sub-model THRSOL002 models the solar radiation on the opaque surface, such as an aluminum plate [27].
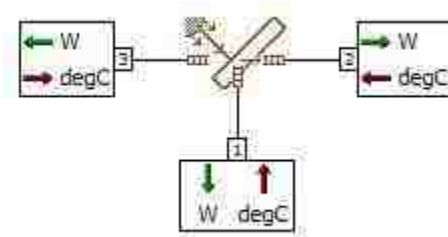

Figure C- 6: AMESim sub-model THROSL001 models the solar radiation on transparent surface, such as glass [27].

C.1 Roof and sunroof

The roof is composed of the external wall, the air gap, and the interior. It is important to include all the heat transfer within this sub-component. First, since the vehicle is moving at a certain speed, there is the convective heat transfer between the ambient air and the roof. To mimic the CCD test environment, constant solar radiation needs to be considered. Then between the roof and the air gap, and between the interior and the air gap, there are heat convections. Also, there is thermal radiation between the roof and the interior. One more energy exchange needs to be taken into account is the thermal radiation between the panel duct and the headliner. Finally, between the interior and the cabin air, there is the heat convection. The corresponding illustration of all the energy transfer is shown below, to show how the model resembles the real situation. The sunroof has a similar configuration, it will not be repeated. Figure C- 7 illustrates the energy transfer process of the roof system.
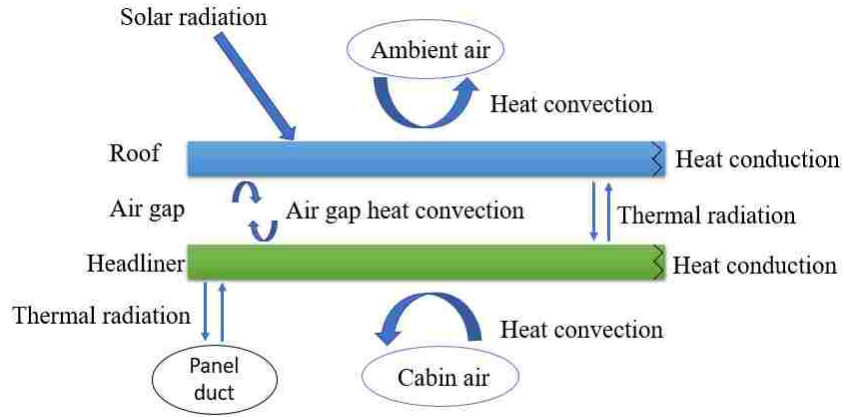
Figure C- 7: An illustration of the heat transfer process in the roof (roof, air gap, and headliner).

C.2 Doors, tailgate, and floor

The doors have a similar configuration to the roof too; they consist of the outer door shell, air gap, and interior. The energy transfer included is heat convection between the ambient air and the outer door shell, the solar radiation, the heat convection between the gap air and the two solid walls, the thermal radiation between the two walls and heat convection between the interior and the cabin air. Since there is no other heat transfer between the surfaces in the doors and other surfaces in the cabin, a relatively simple AMESim configuration is used. The energy transfer illustration of the sub-model can be found in Figure C- 8. The same AMESim sub-model is used to model the tailgate and the floor due to similar configurations of these surfaces in the real car.
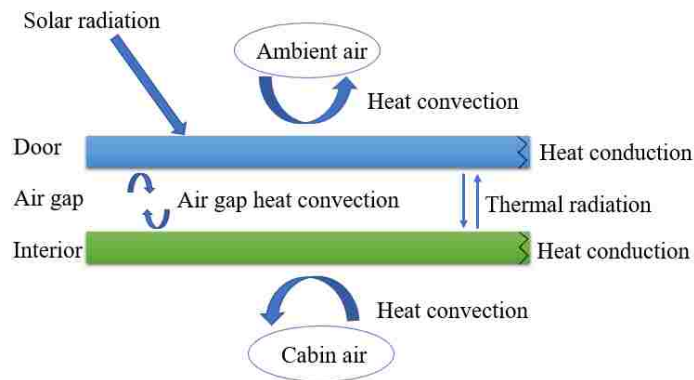
Figure C- 8: An illustration of the heat exchange process in the door (metal surface, air gap, and interior).

81

C.3 Windows and windshield

Windows and the windshield are one-layer surfaces, the energy transfer needs to be considered are the heat convection between the ambient air and the windows, the solar radiation, the heat convection between the cabin air and the windows. Also, since the windows are transparent surfaces, a partial solar load is transmitted and acts as energy gain to the seats. As for windshield, the transmitted solar load is the energy gain to the instrument panel. As shown below, the windows and the windshield thermal masses are constructed in the same way.
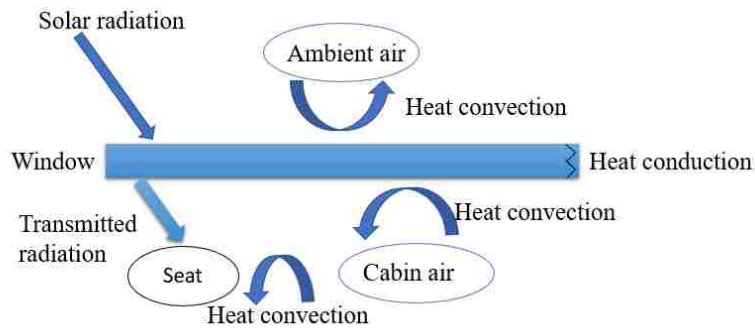
Figure C- 9: An illustration of the heat transfer process in the window.

C.4 Seats and instrument panel

The seats and the instrument panel are simply constructed with one thermal mass individually. For the seats, the heat transfer needs to be taken into account are the heat transfer between the seats and the cabin air through convection, heat gaining from the solar load radiation transmitted through the windows, there is also radiative heat transfer between the seats and the headliner. For the instrument panel, the solar radiation transferred through the windshield is a thermal load on the instrument panel, then there is radiative heat transfer between the panel duct and the instrument panel, as shown in Figure C- 10.
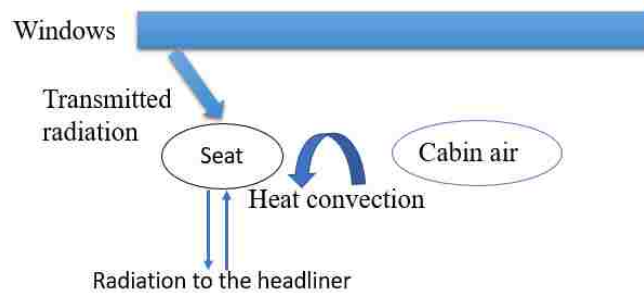
Figure C- 10: An illustration of the heat transfer process in the seats.

82

APPENDIX D CABIN COOL-DOWN TEST

The CCD is a very commonly used standardized experiment to evaluate the AC performance and the human comfort in a vehicle cabin in the automotive industry. Usually, the engineers conduct a series of simulations with this cycle to optimize AC component level design or to model the system level performance and pick the most suitable components. It is a transient cycle, which suggests that the cool-down behavior of the cabin depends on the energy transfer process during the cycle along with time. The vehicle speed of this cycle falls into four segments: constant low speed (25 mph), idle, constant high speed (65 mph) and followed by idle again. The vehicle speed is an input of the AC and cabin model since the vehicle speed affects the external heat transfer between the ambient air and the vehicle wall and it also changes the speed of the front-end air flows into the condenser and hence affects the AC performance. Similarly, the compressor rotary speed is also a user-defined input. Since the compressor is coupled with the engine, it is a function of the engine rpm. Other important ambient conditions are listed in Table D-1.

The cabin is set in recirculation mode during the test, so the amount of air flows into the cabin equals to the air flows back into the evaporators and forms a complete cycle. In the vehicle, the front and rear blowers have seven settings individually which range from the lowest to the highest with five intermediate settings. During the test, the blower is set at its highest power to blow as much air as possible to reach the best cooling performance. The air flow rates are constants at both blower outlets; they are listed in Table D-1. Other properties such as the relative humidity of the air flow at the blower outlet are provided by the cabin model. The air condition at the panel inlets is provided by the AC model. The front-end air flow condition is described by the velocity and temperature maps which are the user-defined inputs of the condenser sub-model. These maps are generated from CFD. Another important input is the compressor efficiency maps. The volumetric efficiency map allows the model to calculate the refrigerant mass flow rate and the isentropic efficiency map allows the model to calculate the enthalpy increase across the compressor. These maps are defined by 2-fdimensional tables which are functions of the compressor rotary speed. These maps are provided by the supplier. Then this cycle is used to calibrate the AC and the cabin model to ensure that the integrated model predicts the correct cabin temperature and compressor power consumption.

The calibrated model allows the engineers to verify the average cabin air temperature, the compressor suction and discharge pressure, and the evaporator inlet and outlet air temperature and so on to evaluate the performance of the model.

Table D- 1: Ambient conditions of the cabin cool-down test (CCD) and city driving test.

Ambient condition	Value
Ambient temperature	43.33°C
Ambient relative humidity	19%
Solar load	1000 W
Front blower air volume flow rate	CFM_{F_Hi}
Rear blower air volume flow rate	CFM_{R_Hi}

Other two transient cycles are used to validate the models; they are city driving cycle and steady-state vehicle speeds cycle. These two cycles are also used to evaluate the AC performance under different conditions. The ambient condition of the city driving cycle is the same as the CCD test. The ambient condition for the other cycle and the vehicle speed maps of both cycles are shown below. The velocity maps are shown in Figure D- 1 and Figure D- 2.

Table D- 2: Ambient conditions of the steady-state vehicle speeds cycle.

Ambient condition	Value
Ambient temperature	48.89°C
Ambient relative humidity	19%
Solar load	1100 W
Front blower air volume flow rate	CFM_{F_Hi}
Rear blower air volume flow rate	CFM_{R_Hi}
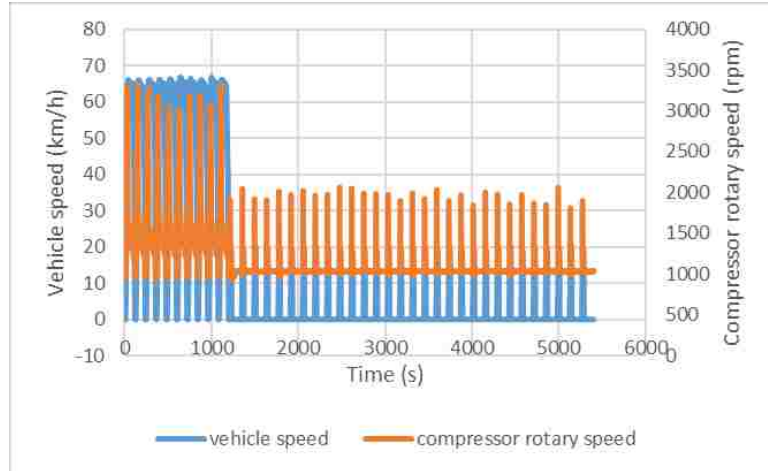
Figure D- 1: The vehicle speed and the compressor speed maps of the city driving test.
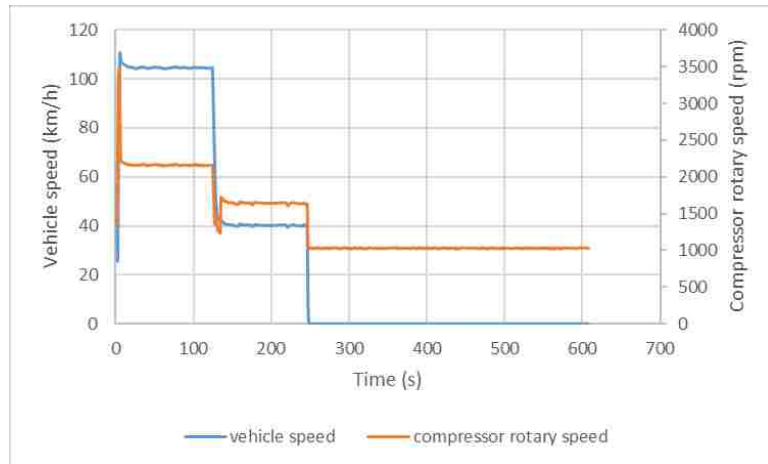
Figure D- 2: The vehicle speed and the compressor speed maps of the steady-state vehicle speeds test.

APPENDIX E   AC MODEL VALIDATION

The whole calibration process started from AC component level calibration. The sub-components of the AC system are calibrated individually with experimental data, and then the cabin model is calibrated separately with the CCD test. Finally, they are integrated to validate the accuracy of the integrated model with another two transient drive cycles.

Validation result for the city driving cycle
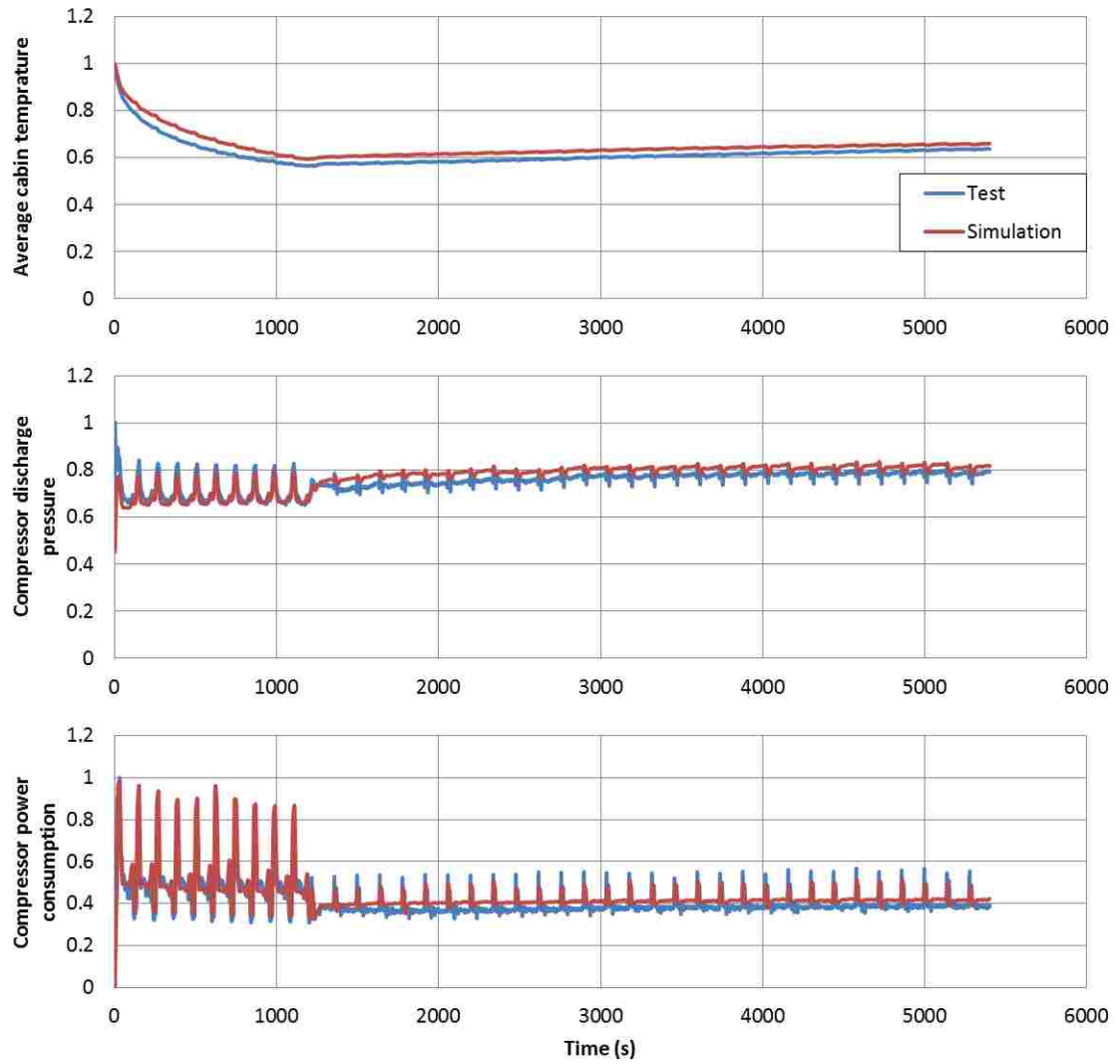
Figure E- 1: The validation results for the city driving cycle, the values are normalized by dividing the data point by the maximum value among that data set.

Validation result for the steady-state speeds cycle
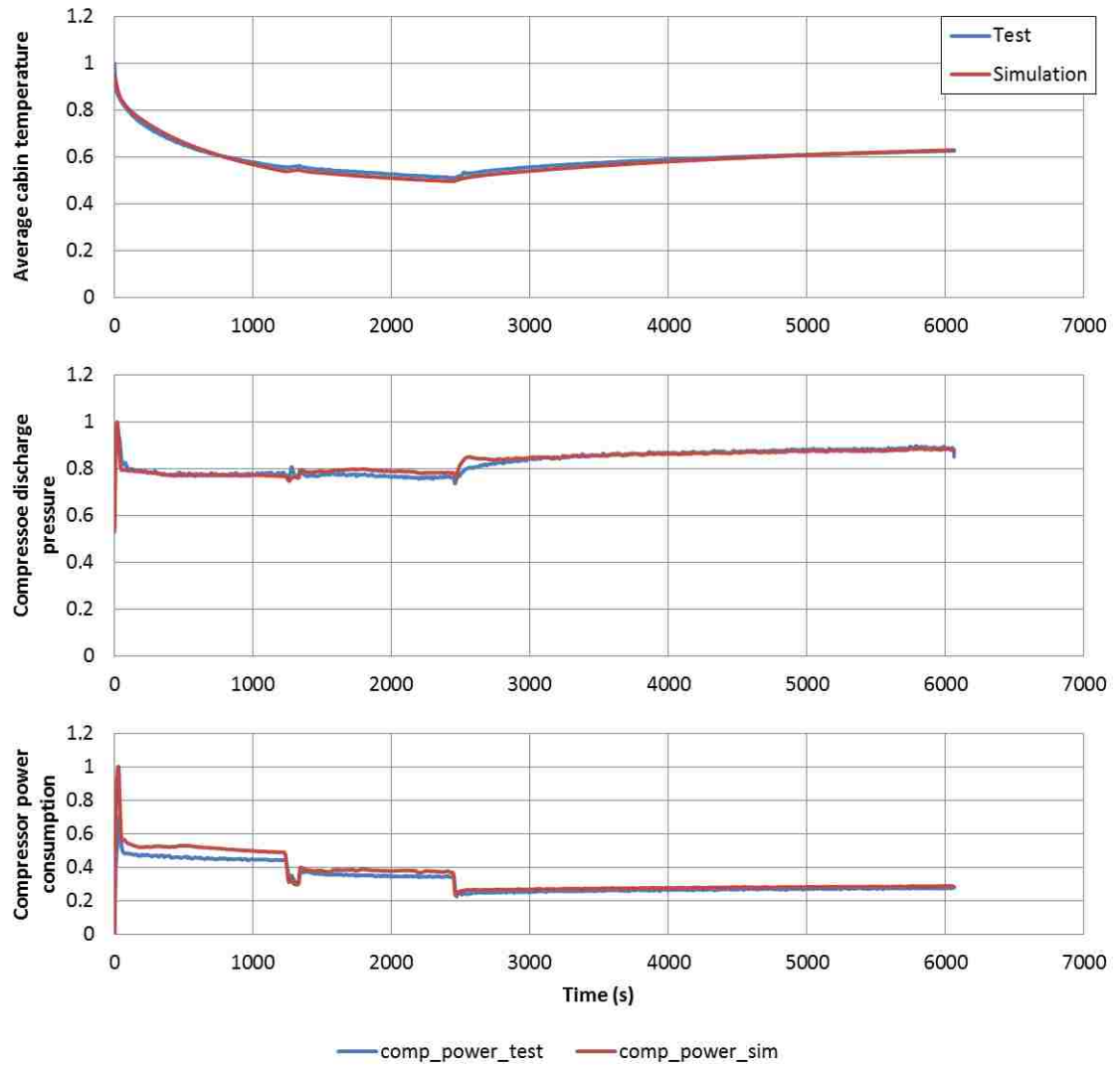
Figure E- 2: The validation result of the average cabin temperature for the steady-state vehicle speeds cycle.

APPENDIX F   WRITTEN PERMISSION

PERMISSION LICENSE: EDUCATIONAL ELECTRONIC USE

Request ID/Invoice Number: KEY783241595-1

Date: July 05, 2018

To: Keyuan Yang

McGraw-Hill Education Material

Author: Cengel and Boles
Title: Thermodynamics: An Engineering Approach
ISBN: 9780073398174
Edition: 8
Description of material: Figure 11-3 on Page 610 and Figure 11-7 on Page 613 (2 Figures ONLY)

Fee: "Waived"

Purpose of Reproduction

Purpose of use: For use in thesis titled 'Impact of Front-end Air Flow Conditions on AC Performance and Real World Fuel Economy'
School: University of Windsor, Canada; Politecnico di Torino, Italy
Professor: David Ting
Number of Copies: 4
Semester: 2018
Format: Print and Electronic (Electronic- open access website).
Distribution: One-time educational use for the above purposes only.

License Number	4382421309545
License date	Jul 05, 2018
Licensed Content Publisher	Elsevier
Licensed Content Publication	International Journal of Refrigeration
Licensed Content Title	Modelling thermostatic expansion valves
Licensed Content Author	Ian W. Eames,Adriano Milazzo,Graeme G. Maidment
Licensed Content Date	Feb 1, 2014
Licensed Content Volume	38
Licensed Content Issue	n/a
Licensed Content Pages	9
Start Page	189
End Page	197
Type of Use	reuse in a thesis/dissertation
Intended publisher of new work	other
Portion	figures/tables/illustrations
Number of figures/tables/illustrations	1
Format	both print and electronic
Are you the author of this Elsevier article?	No
Will you be translating?	No
Original figure numbers	Fig.1
Title of your thesis/dissertation	Impact of Front-end Air Flow Conditions on ◻AC Performance and Real World Fuel Economy
Expected completion date	Sep 2018
Estimated size (number of pages)	150

This Agreement between University of Windsor -- Keyuan Yang ("You") and Elsevier ("Elsevier") consists of your license details and the terms and conditions provided by Elsevier and Copyright Clearance Center.

License Number	4382421249389
License date	Jul 05, 2018
Licensed Content Publisher	Elsevier
Licensed Content Publication	International Journal of Refrigeration
Licensed Content Title	Modeling for multi-pass parallel flow condenser with the effect of refrigerant mal-distribution
Licensed Content Author	Ting Wang,Bo Gu,Bing Wu,Hongtao Ma,Cheng Qian
Licensed Content Date	Dec 1, 2015
Licensed Content Volume	60
Licensed Content Issue	n/a
Licensed Content Pages	13
Start Page	234
End Page	246
Type of Use	reuse in a thesis/dissertation
Portion	figures/tables/illustrations
Number of figures/tables/Illustrations	1
Format	both print and electronic
Are you the author of this Elsevier article?	No
Will you be translating?	No
Original figure numbers	Fig.1
Title of your thesis/dissertation	Impact of Front-end Air Flow Conditions on ⊏AC Performance and Real World Fuel Economy
Expected completion date	Sep 2018
Estimated size (number of pages)	150

VITA AUCTORIS

NAME:	Keyuan Yang
PLACE OF BIRTH:	Wuhan, China
YEAR OF BIRTH:	1993
EDUCATION:	University of Windsor, Windsor, Ontario
	2012-2016 B.Sc
	University of Windsor, Windsor, Ontario
	2016-2018 M.A.Sc